Tuning the Ionic Conductivity of Electrolyte Material to Optimize/Enhance the Solid Oxide Fuel Cell Performance

By

Nabgah Tariq

CIIT/SP22-RPH-008/LHR

MS Thesis

In

MS Physics

COMSATS University Islamabad,
Lahore Campus- Pakistan

Fall 2023

COMSATS University Islamabad, Lahore Campus

Tuning the Ionic Conductivity of Electrolyte Material to Optimize/Enhance the Solid Oxide Fuel Cell Performance

A Thesis Presented to

COMSATS University Islamabad, Lahore Campus

In partial fulfillment

of the requirement for the degree of

MS (Physics)

By

Nabgah Tariq

CIIT/SP22-RPH-008/LHR

Fall 2023

Tuning the Ionic Conductivity of Electrolyte Material to Optimize/Enhance the Solid Oxide Fuel Cell Performance

A Post Graduate Thesis submitted to the Department of Physics as partial fulfillment of the requirement for the award of Degree of MS (Physics).

Name	Registration Number
Nabgah Tariq	CIIT/SP22-RPH-008/LHR

Supervisor

Dr. Ghazanfar Abbas

Associate Professor, Department of Physics

COMSATS University Islamabad,

Lahore Campus

January 2024

Final Approval

This thesis titled

Tuning the Ionic Conductivity of Electrolyte Material to Optimize/Enhance the Solid Oxide Fuel Cell Performance

By

Nabgah Tariq
CIIT/SP22-RPH-008/LHR
Has been approved

For the COMSATS University Islamabad, Lahore Campus

External Examiner: _____

Dr. Amjad Ali
Associate Professor, Department of Physics, University of Okara, Okara

Supervisor: _____

Dr. Ghazanfar Abbas
Associate Professor, Department of Physics, CUI, Lahore Campus

HOD: _____

Prof. Dr. M. Ashfaq Ahmad
HOD, Department of Physics, CUI, Lahore Campus

Declaration

I, Nabgah Tariq, **CIIT/SP22-RPH-008/LHR** hereby declare that I have produced this work, which is presented in this thesis, during the scheduled period of study. I also declare that I have not taken any material from any source except referred to wherever due. If a violation of HEC rules on research project has occurred in this thesis, I shall be liable to punishable action under the plagiarism rules of the HEC.

Date: _____ Signature of the student:

_____

Nabgah Tariq

CIIT/SP22-RPH-008/LHR

Certificate

It is certified that Name of Student, CIIT/SP22-RPH-008/LHR has carried out all the research work related to this thesis under my supervision at the Department of Physics, COMSATS University Islamabad , Lahore Campus and the work fulfills the requirement for award of MS degree.

Date: _____

Supervisor:

_____

Dr.Ghazanfar Abbas
Associate Professors
Department of Physics,
CUI, Lahore.

Head of Department:

_____

Prof. Dr. M. Ashfaq Ahmad
Department of Physics,
CUI, Lahore.

DEDICATION

TO

My FAMILY

Whose support, spiritual guidance, best wishes, and heartfelt prayers create an environment that inspires me to pursue my academic goals.

ACKNOWLEDGMENTS

First of all I would like to bow my head before **"ALMIGHTY ALLAH"**, The Merciful, the beneficent who presented me in a Muslim community and also blessed me with such a lucid intelligence as I could endeavor my services towards this manuscript. Countless salutations are upon the ***HOLY PROPHET MUHAMMAD (May Peace Be upon Him)***, the fountains of knowledge, who guide him "Ummah" to seek knowledge from cradle to grave.

Words are lacking to express my humble obligation to my affectionate, Father (**Tariq Hameed**) my mother (**Yasmeen Tariq**) and my husband (**Muhammad Ashfaq**) for their love, good wishes, inspirations and unceasing prayers for me, without which the present destination would have been more a dream

Under the empathetic guidance, energetic leadership, vigilant pursuit, critical academic analysis, upbeat outlook, and knowledgeable supervision of **Dr. Ghazanfar Abbas**, the work presented in this publication was completed. I am also thankful to **Prof. Dr. Rizwan Raza, Prof. Dr. M. Ashfaq Ahmad & Dr. M. Ajmal Khan** for their moral and intellectual support during my research work at Clean Energy Research Lab (CERL).Their careful inspection and critical feedback enhanced not only my dissertation's quality but also my comprehension of the subject matter in general.

Nabgah Tariq (CIIT/SP22-RPH-008/LH)

Tuning the Ionic Conductivity of Electrolyte Material to Optimize/Enhance the Solid Oxide Fuel Cell Performance

ABSTRACT

The world is using up non-renewable energy sources quickly. Fossil fuel-based energy supplies may run out in a century and two decades. Fossil fuels have many harmful effect on human health and environment. Although fuel cell have received a lot of interest because there great efficiency, simplicity, low impact on the environment, cost effective and fuel adaptability. All fuel cell types, solid oxide fuel cells (SOFCs) is gaining more popularity. Ba-SDC, Sr-SDC, Ca-SDC & Ti-SDC was used as an electrolyte improve properties of solid oxide fuel cell. Due to this purpose electrolyte material was synthesized by co-precipitation method. Prepared material analyzed by various technique such as Raman, UV-Visible, Fourier transform infrared spectroscopy, Conductivity measurement & Open circuit voltage (OCV). Raman sample expose strong peak between 600cm^{-1} to 1200 cm^{-1}, which may be predict the vibration mode and change in structure. It describes the kind of shifting that occur in prepared material. The presence of blue shift in material may be shows heavy atoms in material by which its bound length got shorter and the red shift predict bound length increase by increase by wavelength also it shows the active modes ($F_{1g,}$ A_{1g} and E_g). By UV-visible, synthesized sample's band gap and absorbance are detected. FTIR provides information on the presence of functional groups in materials as well as the organic or inorganic behavior of manufactured materials. With the aid of temperature dependent EIS, the conductivity of materials may be computed. Ti-SDC shows maximum conductivity at 700°C and having value 0.090 S/cm. Using hydrogen as fuel improves the conductivity of materials by utilizing fuel cell performance at temperatures ranging from 500°C to 700°C.

Table of Contents

List of Figures

LIST OF TABLES

Chapter 1

Introduction

1. Introduction

This chapter will cover our discussion about problems due to energy crisis, different sources of energy and also highlight significance of energy.

1.1 Energy crises

Since the birth of industry, the demand for energy has been a significant problem. People used readily available energy resources to determine their needs for energy. Conventional energy sources were more affordable and widely accessible in comparison to renewable energy sources. Science and technological advancements have accelerated industrial growth, which has led to a steady rise in energy demand. About 13000 Mtoe of energy was needed worldwide in 2020, and by 2030, that number is expected to rise to about 17000 Mtoe [1]

As the growing world population, the need for energy is consistently rising. The growth in the population, fast suburbanization, corporate expansion, and other factors, the globe is today facing a vitality crises. Between 2005 and 2030, the world is anticipated to need 50% more energy [2].

In the modern world exponential rise in energy consumption is a result of both rapid population growth and technological advancements, so we utilize energy in many different ways, including for systems in our homes, workplaces, and industries as well as for communication, transportation, and other purposes [3]. The world currently relies entirely on nonrenewable sources of energy, including oil, gas, petroleum, and coal. Additionally, entire globe is now aware of the quick depletion of commodities like coal, gas, and oil [4]. The best possibilities for supplying our energy demands are sources of renewable energy, like wind, biomass, geo thermal, sunlight-based energy, & others, which can be used to generate electricity [5, 6]. Since they are not renewable, sources of energy that are not renewable are also referred to as environmentally friendly energy sources [7]. World energy consumption depending on different energy resources is given Figure 1.1 [8].

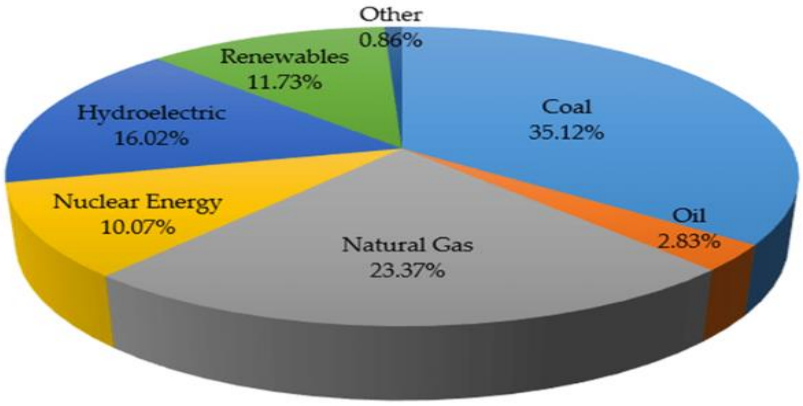

Figure 1. 1 Various sources of power generating worldwide

1.2 Energy storage devices

Energy storage gadgets have drawn a great deal of interest in the modern day due to their quick charging and discharging capabilities and long lifespan [9]. Energy storage devices have been used in a wide range of uses, including energy delivery [10].

According to current trends, more energy storage will likely be needed in the not-too-distant future due to increased energy production and demand, possibly needing power storage for a number of days, weeks, or months [11]. By 2030, estimations predict that the need for power storage will have may become unsustainable. With increasing output and demand, energy storage technologies and equipment have also evolved. The traditional equipment consisted of magnets, batteries, cells and capacitors. Along with modifications to older devices, new technologies have been invented for sustainable and renewable usage [12].

1.3 Devices that convert energy into other forms

Global consumption is rising, which causes a lack of fossil fuels and severe environmental damage. By constructing efficient renewables, the following problems must be solved [13]. One of today's top issues is the creation of energy from sources that are efficient, clean,

and ecologically beneficial. Fuel cell, which provides direct electrical energy conversion from the chemical energy of a fuel. While only produces water and heat as byproducts, may be the best option [14].

1.4 Fuel Cell

In 1838, Sir William Grove created a prototype fuel cell while experimenting with electrolysis of water. Nowadays, fuel cells are becoming more popular because they appear Using hydrogen or other hydrocarbons as a "promising" substitute for conventional fuels is thought to be the most practical and efficient way to address environmental issues. A fuel cell is a one-step energy conversion device that converts chemical energy directly into electrical energy. The electricity produced can be used in the same ways as grid power [15]. Fuel cells produce little hazardous emissions and are environmentally friendly. In comparison to other technologies, the fuel cell operates quietly and generates heat and water. [16]. Many kinds of fuel cells, that all function a little bit differently. Typically, a chemical reaction occurs when hydrogen atoms reach the anode of the fuel cell, causing them to give up their electrons. At this point, the hydrogen atoms have "ionized." Conversely, at the cathode, oxygen enters. Electrolytes are essential in a lot of ways. The only thing that should be permitted to pass among anode and cathode ions. At the anode or cathode, the oxygen and hydrogen ions come together to make water. A fuel cell will produce power if the supply of applied fuels remains at the anodes [17].

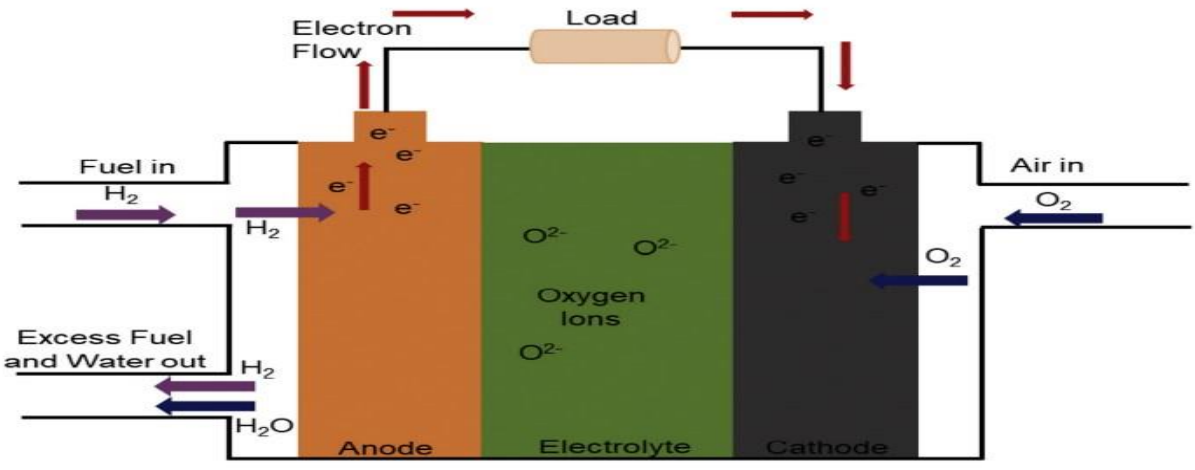

Figure 1. 2 Systematic diagram of fuel cell

1.4.1 Working principle of fuel cell

Fuel cells produce electricity and heat through the electro chemical process known as inverted electrolysis. This takes place as water as by product. A collection of current fuel cell concepts is provided below; nonetheless, they all operate according to the same fundamental tenet [18].

At anode:

In the prescience of catalyst and hydrogen fuel, Oxidation occurs and protons and electrons are formed

$$2H_2 \longrightarrow 4H^+ + 4e^-$$

At Cathode:

The Formation of water as chemical reaction occur with oxygen when electrons and protons interact as shown

$$O_2 + 4H^+ \longrightarrow 2H_2O$$

Net Reaction:

$$2H_2 + O_2 \longrightarrow 2H_2O$$

1.5 Types of fuel cell

Operating temperatures, productivity, applications, and cost are all different for the various kind of fuel cells. In accordance with the type of fuel and electrolyte utilized, they are categorized into six large classes [19].

- Alkaline fuel cell (AFC)
- Phosphoric acid fuel cell (PAFC)
- Molten carbonate fuel cell (MCFC)
- Proton exchange membrane fuel cell (PEMFC)
- Direct methanol fuel cell (DMFC)
- Solid oxide fuel cell (SOFC)

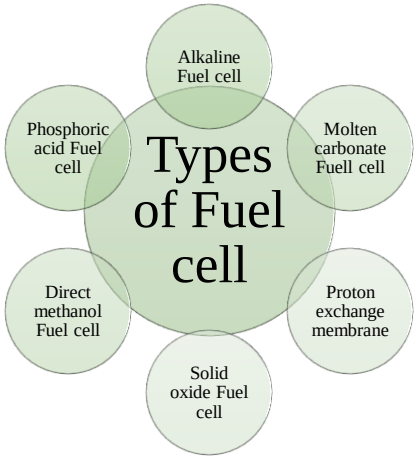

Figure 1. 3 Types of Fuel Cell

1.5.1 Alkaline fuel cell

Utilizing potassium hydroxide (KOH), an alkaline electrolyte, in a water-based combination, the AFC produces energy. Because hydroxyl ions are present and moving through the electrolyte, it is feasible to form a circuit and use up electrical energy. At the anode, four negatively charged hydroxyl ions and two hydrogen ions unite to form four water molecules and four electrons. [20]. A reaction between oxidation and reduction is occurring.

$$2H_2 + 4OH^- \rightarrow 4H_2O + 4e^- \quad \text{(Oxidation)}$$

The electrons in the aforementioned reaction use an external circuit to react and reach the Cathode. By interacting with water, it also produces (OH^-) ions. The cathode side saw the Combination of two water molecules with two oxygen molecules as well as the absorption Of four e- ions from the negatively charged Hydroxyl ions.

$$O_2 + 2H_2O + 4e^- \rightarrow 4OH^- \quad \text{(Reduction)}$$

Temperatures between 60°C and 90°C are used to run alkaline fuel cells. According to recent research, the AFC is currently run between 23°C to 70°C. Because of this lower operating temperature, the AFC is also regarded as a fuel cell with low operating temperature and inexpensive catalysts [21].The most popular catalyst for accelerating the electrochemical process is nickel, which is utilized on side anode and side cathode. AFCs

have more than 80% CHP efficiency and about 60% electrical efficiency. AFCs could produce more than 20KW of electricity.

1.5.2 Phosphoric acid fuel cell

The liquid phosphoric acid (H_3PO_4) acts as the fuel cell's electrolyte in phosphoric acid (PAFC), which also use carbon paper as an electrode. The operating range (PAFC) is between 150°C and 220°C temperature because ionic conductivity of phosphoric acid is poor at the low temperature. Charge carrier in PAFC is a hydrogen ion, which moves through anode electrodes to the cathode electrode by an electrolyte material. An outer circuit creates an electrical current from the released electrons, which then return to the cathode [22].

$$2H_2 \rightarrow 4H^+ + 4e^- \qquad \text{(Oxidation)}$$

$$O_2 + 4H+ + 4e^- \rightarrow 2H_2O \qquad \text{(Reduction)}$$

1.5.3 Molten carbonate fuel cell

The fuel cell that operate at very high temperatures in which include molten carbonate fuel cells (MCFCs). A beta alumina solid electrolyte inert ceramic matrix is used as the suspended porous electrolyte in molten carbonate fuel cell. The optimum temperature for operation of MCFC is 650 °C, this is the typical temperature at high power [23].

$$H_2 + CO_3^{2-} \rightarrow H_2O + CO_2 + 2e^- \qquad \text{(Oxidation)}$$

$$(1/2)\ O_2 + CO_2 + 2e- \rightarrow CO_3^{2-} \qquad \text{(Reduction)}$$

1.5.4 Proton exchange membrane fuel cell

In proton Exchange membrane fuel cell, at anode side, the electron is expelled and hydrogen is catalyzed to create a proton ion. While the proton travels across the membrane, the electron travels via the external circuit and produces electricity. This fuel cell uses free hydrogen as an impurity on anode side, and electrolyte in these cells is made up of acid polymers. PEMFC efficiency is from 40 to 50 percent when operated below 100°C [24]. Automobiles employ PEMFC.

$$H_2\ (g) \rightarrow 2H^+ + 2e^- \qquad \text{(Oxidation)}$$

$$(1/2)\ O_2\ (g) + 2H^+ + 2e^- \rightarrow H_2O\ (l) \qquad \text{(Reduction)}$$

1.5.5 Direct methanol fuel cell

In direct methanol fuel cell (DMFC) systems employ methanol as their energy source. Water or steam is created at the cathode side utilizing airborne oxygen, whereas methanol is transformed into carbon dioxide (CO2) at the anode side. Operating at a temperature of 60°C, DMFCs have an efficiency of 55–60%. This kind of fuel cell is utilized in portable equipment [25].

$$CH_3OH + H_2O \rightarrow CO_2 + 6H^+ + 6e^- \quad \text{(Oxidation)}$$

$$(3/2)\ O_2 + 6e^- + 6H^+ \rightarrow 3H_2O \quad \text{(Reduction)}$$

1.5.6 Solid oxide fuel cell

In solid oxide fuel cell (SOFC) electrolyte made of the solid ceramic substance condense yttria stabilized zirconia is what they employ. The water is concurrently produced in the fuel cell when hydrogen and oxygen are combined. As a consequence, SOFC operates at an extremely high temperature. The device is used to produce energy at temperatures between 800 and 1000 °C. The solid oxide fuel cell's efficiency, which ranges from 50 to 60 percent, is one of its main advantages while running at high temperatures. Since it has internal reforming capabilities, it does not

Cogeneration, heat that is wasted can be recycled to create more energy. [26].

At the anode and the cathode, the overall response is as follows:

$$H_2 + O^{2-} \rightarrow H_2O + 2e^- \quad \text{(Oxidation)}$$

$$(1/2)\ O_2 + 2e^- \rightarrow O^{2-} \quad \text{(Reduction)}$$

1.6 Working of SOFC

Cathode, anode, and electrolyte are three of the different types of materials utilized in SOFC production. The electrolyte is sandwiched between the cathode and anode electrodes.. It is built in a thick manner. Air is utilized to fuel from a different side, such as the anode, across the cathode. The provided fuel was split into (H^+) and (e^-). These (e-) are powered by an external circuit. The splitting of oxygen into oxygen ions (O_2^-) occurs similarly. These (O_2^-) travel by the electrolyte and arrive at the cathode where water is the

result of their combination with hydrogen ions. Figure (1.4) illustrates how the SOFC operates. [27].

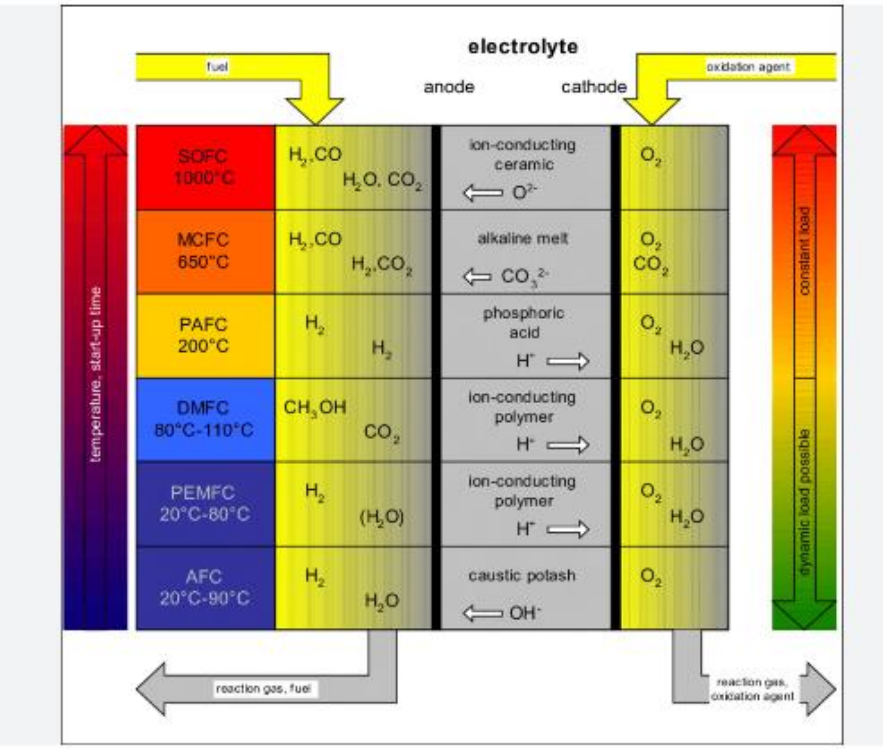

Figure 1. 4 All types of fuel cell

1.7 Components of SOFC

The cathode, anode, and electrolytes are the three primary components of a solid-oxide fuel cell (SOFC). Which are two electrodes and an electrolyte respectively. For effective electricity generation, these parts need to have a few characteristics, such as great chemical/physical reliability, chemical stability between them, robust mechanical strength, enough thermal expansion to prevent cell cracking, and being reasonably priced [28].

1.7.1 Anode

The anode acts as the SOFC's negative electrode, transporting electrons and distributing fuel equally throughout the entire body. The anode structural system's porosity, which guarantees fuel passage at the catalyst surface, is another crucial element. The anode is

typically created with 20% to 40% porosity to allow for gas supply. Chemical compatibility of the anode, which means it must not react with connectors or electrolytes at high temperatures, is another crucial consideration. In this context, nickel-yttria-stabilized zirconia (Ni-YSZ), which also serves electrolyte in SOFCs, is frequently utilized as an anode [29]. Nickel performs effectively because of its superior catalytic abilities and strong conductivity.

Nickel performs effectively and is regarded as the best material for making anodes because of its strong ionic conductivity and extraordinary catalytic properties. Due to its minimal operating temperature and exceptional chemical and physical characteristics, Ni-GDC is attracting a lot of attention. GDC is utilized as an electrolyte material. The performance of this kind of manufacturing is excellent at low working temperatures [30]. Anode has following characteristics.

- ¶ It is a mixed conductor
- ¶ Electrolyte compatible thermal expansion coefficient.
- ¶ Chemical and physical stability in a reducing environment operating temperature.
- ¶ Strong catalytic power to oxidize the fuel cell.
- ¶ Anode is very cost effective and affordable material.

1.7.2 Cathode

O_2 is reduced at the cathode, where this produces oxygen ions. Since O_2 reduction requires strong catalytic activity, the cathode is required [31]. Similar to the anode, the cathode requires good chemical compatibility with other fuel cell components and just right amount of porosity to allow O_2 gas to flow. Strontium-doped lanthanum manganite is one of the perovskite-based materials that is frequently utilized as a cathode in SOFCs. As with the YSZ electrolyte, the LSM's thermal expansion coefficient is comparable, and it has an outstanding electrical conductivity of 100 S/cm1 at 600 °C. Since no other components for the SOFC were disclosed at first, the cathode was constructed of platinum. The cost of making cells rises, though, when platinum is used. For SOFC commercialization, this was a roadblock. . As a result, the perovskite of the AbO_3 type was later found and employed as cathode materials. These materials seem appropriate because they were created by combining conductivity [32].

A cathode material that meets these criteria is described.

- ¶ Cathode should be increase oxygen reduction reaction.
- ¶ Low cost and simple to synthesize.
- ¶ Reduce polarization resistance.
- ¶ Thermal expansion coefficient must be compatible.
- ¶ Rapid chemical reaction to reduce oxygen level.

1.7.3 Electrolyte

The most crucial element of a fuel cell is its electrolyte, and different fuel cell types are classified based on the kind of electrolyte they use. For instance, while the electrolyte is used in polymer membrane in PEMFC, it is used in solid form in SOFC. The SOFC serves as an extractor between oxidant and fuel in order to avoid spread electrons throughout device. Due to distribution of electrons, the ohmic losses inside the electrolyte rise, resulting in a fall in SOFC efficiency. To achieve the redox reaction with fuel, the electrolyte must also have extremely high ionic conductivity as the oxide ions (or proton) travel across it [33]. Another important characteristic of an electrolyte is its chemical compatibility. Its redox reaction inertness and chemical compatibility correspondingly with the anode and cathode electrodes. The most common electrolyte component used in SOFCs is yttria-stabilized zirconia, or YSZ. exceptional stability, outstanding mechanical qualities, and high ionic conductivity at high temperatures (800°C–1000°C) are all features of the YSZ [34]. Gadolinium-doped ceria (GDC), which enables low temperature operation for SOFC, also exhibits exceptional electrolytic characteristics. . Some requirements in electrolyte are following.

- ¶ It would be firm ionic conductor.
- ¶ It ought to be an electronic insulator.
- ¶ Its synthesis should make use of low cast ingredients.
- ¶ It must have a dense construction to halt the passage of gases.

1.8 Fuel for SOFC

Several solid oxide fuel cell-related fuels are nearby.

1.8.1 Biogas as fuel

A green energy source is biogas. It also applies to highly pure methane. For heating, methane that has a high degree of purity is a fantastic, sustainable fuel. During fuel cell testing, biogas is used as the input fuel at the electrodes. Biogas is created during the breakdown of organic materials. It is made up of a variety of gases, primarily methane (CH_4 50–70%), carbon dioxide (30–50%), oxygen (O_2), nitrogen (N_2), and very small amounts of water & hydrogen sulfide [35].

1.8.2 Natural Gas (CH_4)

Despite being readily available, it is preferable to avoid consuming these fuels because doing so harms cells.

1.8.3 Methanol (CH_3OH)

Methanol is abundantly available, however it shouldn't be used because it harms cells when it burns because of the carbon that is produced.

1.8.4 Ethanol (C_2H_6O)

Ethanol can be handled, transported, and stored with ease.

1.8.5 Hydrogen

The best fuel for SOFC is hydrogen (H_2), however issues with hydrogen manufacturing, transportation, and storage limit its availability.

1.9 Advantage of SOFC

Compared to other fuel cell types and other energy generating techniques, SOFC has a number of advantages. In contrast to other fuel cell types that use a fluid electrolyte, electrolyte upkeep in a SOFC lower because it is solid. Furthermore, there is little chance that evaporation will change the chemical makeup of the materials used as electrolytes. It is entirely prevented that other SOFC components will degrade as a result of solid

electrolytes. Being able to offer several cell designs, including tubular or planar forms, is another important benefit of SOFC. This is because every component of the cell is made of solid. Another benefit of the SOFC is that it has a 70% efficiency rating, which exceed that of nearby power plants. Electricity can be produced using waste heat. Steam is produced as a byproduct of the electrochemical reaction in fuel cells, hence no additional water arrangements are needed. Due to the extremely thinness of SOFC components, internal component resistance and total cost are decreased. The SOFC runs at a very high temperature between 700 and 1000 ^{o}C, which causes the electrode reactions to happen very quickly. The SOFC can also burn a variety of hydrocarbons because it runs at high temperatures. Because SOFC don't require extensive fuel purification, they may be distinguished from other forms of fuel cells.

1.10 Challenges of the SOFC

Since the operating temperature is higher & the cost production is significantly greater, SOFC has limitations in commercial applications. The cost of the materials to be used is considerably increased by the constraint on their capacity to tolerate such high temperatures. Due to this, SOFC fuel cells now cost more overall. As a result of the requirements that these materials must meet, like being able to withstand an oxidizing or reducing environment. Due to the lengthy startup and cooling times required by high working temperatures, it is less dependable. Starting up and cooling down procedures become unusable under thermal stress. This temperature requires excessively high maintenance costs for the SOFC [36].

1.11 Applications of SOFC

The following are some of the varied uses of fuel cells.

- Fuel cells are used in portable electronics like radios and cellphones.
- It is used in all kind of transportation machinery, such as buses, Automobiles, trucks, ships, and aircraft.
- It is utilized in stationary power generation plants in European nations.
- It is employed by soldiers in submarines, airplanes, tanks, and missiles.

1.12 Objectives of SOFC

- Samples (Ba-SDC, Sr-SDC, Ca-SDC and Ti-SDC) will be prepared by co-precipitation method.
- By fine-tuning the band gab, the activity of the electrolyte may be boosted.
- Material will be characterized by Raman spectroscopy.
- • Using SEM and XRD analysis as tools, the structural investigation will be completed.
- UV-VIS is used to calculate the band separation.
- In this study, the structural, thermal, and chemical aspects will be focused in order to enhance fuel cell efficiency at low temperatures.
- Electrochemical characteristics of functional Nano-composites will be determined.

Chapter 2

Literature survey

2.1 Somoju Ramesh *et al.* (2023). In the current work, the system of compositions MySmxyCe1xO2 (M = Al, Ca, Mg, & Sr, x = 0.20; y = 0.025) is examined as an electrolyte for IT-SOFCs. Samples are made using sucrose-pectin-modified low the temperature sol-gel technique to create a nano crystalline powder. At 600 °C, the produced nano crystalline powder was calcined. The typical size of a crystallite is between 11 to16 neno meters. The co-dopants Al, Ca, Mg, and Sr help the SDC 20 become denser at the temperature of sintering that are substantially lower (1300 °C). XRD, a method for characterizing these samples impedance spectroscopy, Raman, UV-Visible, FESEM, and Williamson-Hall plots. A power source Temperatures between 300 and 700 °C are used to measure conductivity. The compositional sample at 700°C, $Sr_{0.025}Sm_{0.175}Ce_{0.80}O_2$ (SrSDC) has a greater conductivity of electrical is 0.03342 S/cm. [37]

2.2 Faizah Altaf *et al.* (2019). Using co-precipitation technique, the BGC ($Ba_{0.10}Ga_{0.10}Ce_{0.80}O_{3-\delta}$) the electrolyte component was created. The substance had cubic fluorite crystal shaped with 36 nm size. It was discovered that the electrolyte substance has a conductivity of 0.071 S/cm. At 650°C and utilizing hydrogen as the fuel, Maximum power density and current were 893mAcm^{-2} and 375W/cm^2, respectively [38].

2.3 Mao Zongqiang *et al*. (2012). Low temperature anode support research The SDC electrolyte-based SOFC has been developed. SDC electrolyte was printed on a green piece after anode support was created using an SDC 50 weight percent NiO slurry. It was dried at 90°C for 14 hours & then sintered at 1350°C for 10 hours. The electrolyte film on the bilayer is flat, dense, and free of any cracks, according to SEM images. The film was 12 mm thick. The cell was tested between 450 and 600 °C. 0.94V is the OCV. 797mV/cm^2 of power density utilizing air and H_2 [39].

2.4 M. Ajmal Khan *et al.* (2013). The applications of Solid oxide fuel cell requiring low and intermediate temperatures provide a lot of room for ceria-based electrolyte materials. Three different kinds of ceria based nano composite electrolytes (LNK-SDC, LN-SDC, and NK-SDC) were created in the current study. The produced ceria-based nano-composite electrolyte materials were characterized using a variety of techniques and a one-step co-precipitation approach. The temperature impact, the materials' in shape, and their crystal structure were examined using by TGA, XRD, and SEM. All composite electrolytes have been found to include cubic fluorite structures. Additionally, using the Scherrer formula,

sizes of crystallites in the LN-SDC, NK-SDC, and LNK-SDC were identified to be in range from 19, 20 and 21 nm, respectively. These numbers highlight a solid in agreement with the SEM findings. The electrochemical Impedance Spectroscopy (EIS) with a two probe approach was used to measure the ionic conductivities, moreover, the activation energies also were computed using an Arrhenius plot. LiCuZnNi oxide electrodes were used to attain the greatest power density of 484 mW/cm^2 of LNK-SDC electrolyte at the 570 °C [40].

2.5 Asia Rafique *et al*. (2020). Two different phase nano composite electrolytes created at low temperature solid oxide fuel cells (LT-SOFCs) are being compared. Doped ceria shown high oxide ion moveability for LT-SOFCs is covered with various oxides to create the nano composites. These brand-new co-precipitated two phases of nano composite oxide ionic conduct (MCe0.8Sm0.2O2-MO2, where M = Zn^{2+}/$Ba^{2+/}La^{3+}$/Zr^{2+}/Al^{3+}) were made. Ionic conductivities were evaluated using DC conductivity, & electrochemical impedance spectroscopy (EIS) was use for analyze to interface studies between these two phases. By using of X-ray diffraction (XRD) and scanning electron microscopy tool (SEM), structural characteristics of nano composite electrolytes were investigated. Thermo gravimetric analysis technique (TGA) and differential scanning calorimetry (DSC) were used to examine the thermal stability. The Zn-SDC based cell demonstrated the highest performance of 590 mW/cm2 at 550 °C, while the coated samples for the Ba-SDC, La-SDC, Zr-SDC, and Al-SDC based cells displayed values of 550 mW/cm^2, 540 mW/cm^2, 450 mW/cm^2, and 340 mW/cm^2, correspondingly, with hydrogen as a fuel. In order to overcome the difficulties of the solid oxide fuel cells (SOFC), coated-SDC based nano composite materials are aviable option for decreasing the temperature at which machine operates [41].

2.6 Mingfei Liu *et al.* (2012). In solid oxide fuel cells operating at intermediate temperatures, as an electrolyte material (IT-SOFCs), doped ceria has received much research. Although records of elevated peak power densities exist, electronic conductivity of doped ceria under fuel cell working circumstances decreases the open circuit voltage (OCV) and consequently energy efficiency, particularly with thinner electrolyte membranes at higher operating temperatures. We present a novel cell structure that consists of a thin SDC electrolyte membrane supported by a composite anode made of the mixed-

ion conductors $BaZr_{0.1}Ce_{0.7}Y_{0.1}Yb_{0.1}O_3$ (BZCYYb) and NiO. A thin layer of doped barium cerate and zirconate is formed at the interface by the inter-diffusion of BZCYYb and SDC during co-firing. This layer limits SDC's electronic conduction and enhances OCV and cell performance. [42].

2.7 Yifeng Zheng *et al.* (2011). $Ce_{0.8}Sm_{0.2}O_{1.9}$ (SDC) examined to determine the impact of Sr addition (0–10 mol%) on densification, ionic conductivity, thermal expansion, flexural strength, and crystal structure. Sr addition improves densification and lowers sintering temperature by around 100 °C. All of the samples have a fluorite structure, according to X-ray diffraction examination. Impedance spectroscopy tests showed SDC with adequate ratio of Sr (4–10 mol%) has stronger ionic conductivity and lower activation energy of SDC. The sample reaches the greatest ionic conductivity, which is around 30% greater than that of SDC at 700 °C, Sr added increases up to 6 mol% (0.94SDC-0.06Sr). In addition, flexural strength rises with Sr content, rising from 97 to 160 MPa for SDC with the addition of 10 mol% Sr. Additionally, all of samples' thermal expansion linear. The thermal expansion coefficient is barely affected by addition of Sr [43].

2.8 Yuan Ji *et al.* (2005). Ceria that has been laced with Samaria The glycine nitrate technique was used to create $Ce_{0.9}Sm_{0.1}O_{1.95}$ (SDC) and samaria and praseodymium co-doped ceria $Ce_{0.9}Sm_{0.08}Pr_{0.02}O_{1.95}$ (SPDC) powders. The appropriate powders used to press pellet & sinter them in air at 1400 °C to create SDC & SPDC electrolytes. The electrolytes not thick, & SPDC more porous than SDC, according to SEM and open porosity measurements. Oxygen vacancy concentration of SPDC was found to be greater than SDC, according to Raman spectra. Development and testing of solid oxide fuel cells (SOFCs) using SPDC & SDC electrolytes. SOFC with SPDC electrolyte has a better power density but a lower open circuit voltage. The SOFCs' open circuit impedance was measured, results revealed that the SPDC electrolyte's polarization and Ohmic resistances are lower than those SDC electrolyte. By altering the grain boundary conditions to allow for more oxygen vacancies to exist and move more quickly, it is explained that co-doping Pr in Sm-doped ceria may boost the oxygen ionic conductivity. A significant factor in reducing polarization of the electrolyte-electrode interface of SOFCs may be played by Pr's electrochemical catalytic activity [44].

2.9 Jihai Cheng *et al.* (2019). By using the sol-gel process, ceria-based electrolyte powders ($Ce_{0.8}Sm_{0.2x}Fe_xO_2$) with double-doped Fe_2O_3 and Sm_2O_3 were created. It has been investigated how the electrolyte materials are structured and electrochemically behave. X-ray diffraction analysis (XRD) was used to investigate how precursor powders phase formed. The sintered electrolyte discs were subjected to sinterability and microstructural measurements. Estimating the electrochemical characteristics was done using electrochemical impedance spectroscopy (EIS). As a result of being the formation of crystalline cubic fuorite when calcined at 700 °C, according to the findings. The x=0.1 sample might yield a total conductivity of 0.0263 S cm^{-1}. According to the electrochemical analysis results, which demonstrated that $Ce_{0.8}Sm_{0.2}O_{1.9}$ (SDC) electrolytes supplemented with specific Fe_2O_3 had good electrical characteristics [45].

2.10 Saddam Hussain *et al.* (2021). With the co-precipitation approach and different ZnO:SDC weight ratios, we synthesize samarium-doped ceria (SDC) nanocomposite electrolytes in this study for use in solid oxide fuel cells. Thermo gravimetric analysis (TGA), differential scanning calorimetry (DSC), X-ray photoelectron spectroscopy (XPS), and scanning electron microscopy (SEM) are used to characterize the physicochemical properties of the nanocomposite electrolytes. To assess the electrical characteristics of the electrolytes, electrochemical impedance spectroscopy is used. The results suggest that the ZnO (x=0.2) nanocomposite with the best composition exhibit a greater ionic conductivity of 0.1–0.7 S/cm at 350–700 °C. Hydrogen is used as the fuel to gauge the electrolyte performance of the ZnO/SDC nanocomposite fuel cells. ZnO nanocomposite material (x=0.2) has power density of 804 mW/cm^2 and a maximum open-circuit voltage (OCV) of 1.10 V at 700 °C as-synthesized [46].

2.11 Meng Xia *et al.* (2018). By mechanical mixing, a composite of co-doped barium cerate ($BaZr_{0.1}Ce_{0.7}Y_{0.1}Yb_{0.1}O3_{-\delta}$, BZCYYb) and samarium doped ceria ($Sm_{0.2}Ce_{0.8}O_{2-\delta}$, SDC) is created, and it is tested as an electrolyte for intermediate temperature solid oxide fuel cells (IT-SOFCs. After five hours of sintering at 1500 °C, the coexistence of SDC and BZCYYb in the composite electrolyte is found by means of X-ray diffraction. Modest deflection of the diffraction peak indicates element transport between the two phases. Findings from the scanning electron microscope and electron probe micro analyzer show that small BZCYYb grains scatter equally around the SDC grain, restricting the growth

SDC grains and reducing average grain size of composite electrolyte. According to an impedance spectroscopy experiment, adding 15–30 weight percent of BZCYYb to SDC can dramatically lower grain boundary resistance by nearly an order of magnitude. Utilizing perovskite ($La_{0.6}Sr_{0.4}Co_{0.2}Fe_{0.8}O3_{-\delta}$, LSCF) cathode and nickel cermet (Ni-SDC) anode, creation of individual cells using the composite electrolyte [47].

2.12 Kadi Tamm *et al.* (2013). By using an infiltration technique and altering the microstructure of a porous $Ce_{0.85}Sm_{0.15}O_{2-\delta}$ based scaffold, three distinct single solid oxide fuel cells were created. The cathode was made of $La_{0.8}Sr_{0.2}CoO_{3-\delta}$, and the anode was made of $La_{0.3}Sr_{0.7}VO_{3-\delta}$, which was activated using CeO_2 and Pd nanoparticles. Modified FIB-SEM was used to analyze the microstructure of the porous $Ce_{0.85}Sm_{0.15}O_{2-\delta}$ based scaffolds. Humidified hydrogen as the fuel, a single cell operating at 873 K and having the best electrolyte framework and scaffold porosity displayed the best power density value of 320 mW cm^{-2}. Contrarily, single cell that used humidified methane as the fuel had best power density value, measuring 175 mW cm^{-2} at 873 K, despite having larger $Ce_{0.85}Sm_{0.15}O_{2-\delta}$ particles and somewhat lower scaffold porosity overall[48].

2.13 Chin-Tien Shen *et al.* (2019). Look at how characteristics yttrium-stabilized zirconia (YSZ) electrolyte are affected by the addition of titanium dioxide (TiO_2) & samarium doped cerium oxide (SDC). Investigations are conducted electrolyte's microstructure, mechanical, and electrochemical properties. Supplying carbon dioxide to the Ni-YSZ electrode and nitrogen to the LSM electrode allows for the measurement of CO_2 electrolysis performance. The inclusion of SDC and TiO_2 can improve grain size and lower sintering temperature, according to the results. At 1000 °C, the ionic conductivity is 0.123 S cm^{-1}. A further factor is that at 1000 °C, the thermal expansion coefficient is 8.25 106 K^{-1}. In a solid oxide electrolysis cell, the cell's current density measures at 439 mA cm2 at 1.3 V and 1000 °C [49].

Chapter 3

Experimental Methodology

3.1 Material and Experimental Procedure

This chapter will go over my research's experimental methodology. We can synthesized our material by different methods including sol-gel, hydrothermal, co-precipitation and solid state reactions but we synthesized our material by co-precipitation method to take pure, dense and homogenous material as well as the process of nucleation growth and agglomeration all occur simultaneously.

1st synthesized Ba-SDC.

2nd synthesized Sr-SDC.

3rd synthesized Ca-SDC.

4th synthesized Ti-SDC.

Chemicals Name	**Chemicals Formula**	**Chemicals Molecular Weight (g / mol)**
De ionized water	H_2O	18.015
Cerium nitrates hex hydrate	$Ce(NO_3)_3.6H_2O$	434.22
Samarium nitrate hex hydrate	Sm (NO3)3. $6H_2O$	444.47
Barium nitrate	$Ba(NO_{3)2}$	261.34
Strontium nitrate	$Sr(NO_3)_3$	211.63
Calcium nitrate tetra hydrate	$Ca(NO_3)_3.4H_2O$	236.15
Titanium dioxide	TiO_2	79.865
Sulphric acid	H_2SO_4	98.079
Sodium carbonate	Na_2CO_3	105.99

Table 3. 1 Chemical that used, formula & molecular weight

3.2 Equipment

- Aluminum foil
- weighing balance
- Beakers
- Magnetic stirrer
- Blow drier
- Mortar pestle
- Spatula
- Pasteur pipette
- Filter paper
- Vacuum filtration pump
- Drying oven
- Porcelain crucible
- Furnace
- Hydraulic press
- Silver paste
- Coating brush
- Combustion boat
- Petri dish
- Magnetic bar

3.3 Safety equipment

- Latex Gloves
- Safety goggles
- Lab coat
- Caps
- Face mask
- Tissue paper

3.4 Calculation

The Co-precipitation process is used to create the electrolyte material. The calculations were only done for 20g of the entire sample weight in order to keep the samples affordable.

3.5 Synthesis of material (Ba-SDC, Sr-SDC, Ca-SDC &Ti-SDC)

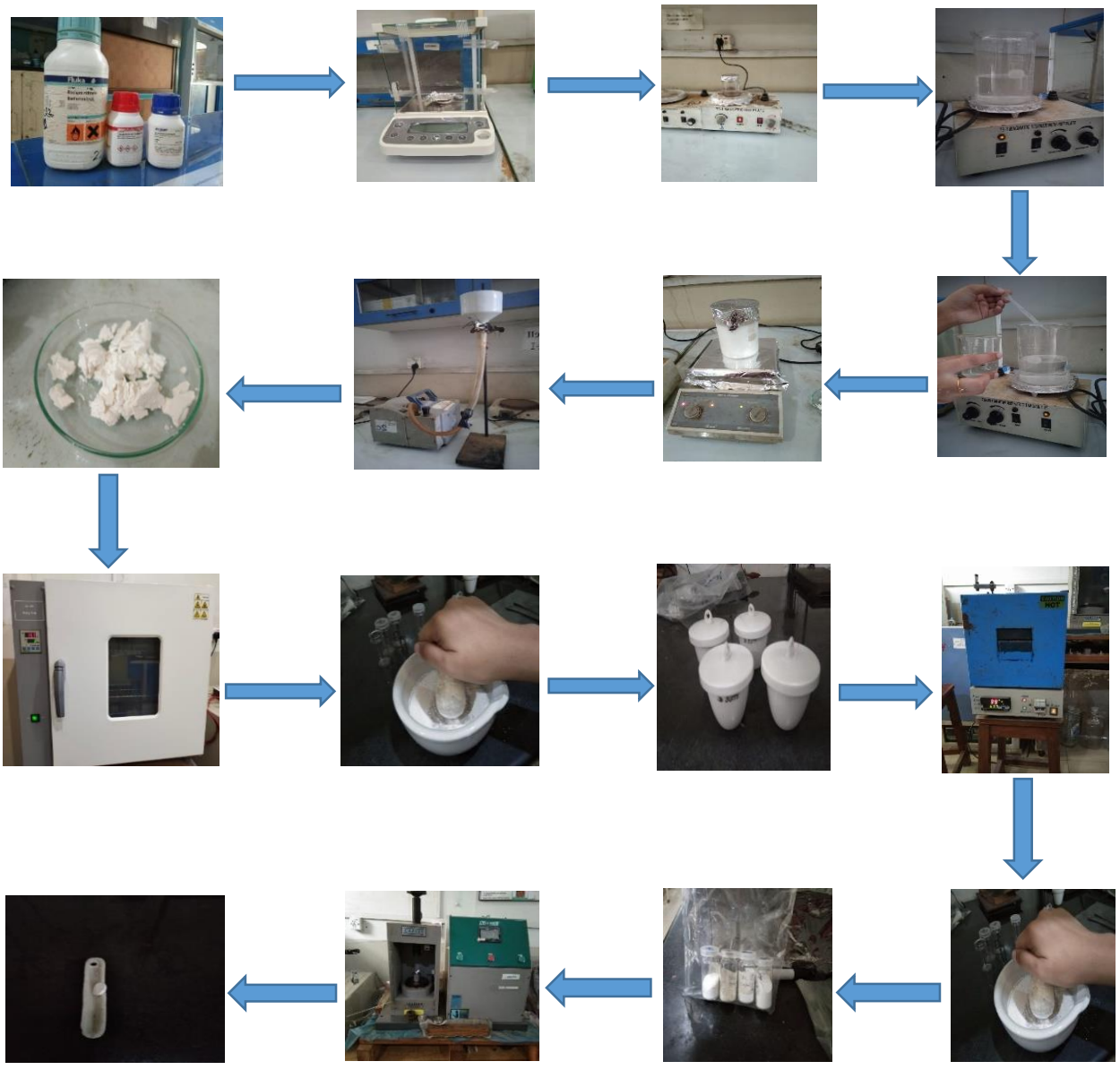

Figure 3. 1 Schematic diagram of experimental process

3.6 Experimental procedure for Ba-SDC

Barium, samarium co-doped Cerium Oxide electrolyte material SOFC was successfully produced by the co-precipitation process. The following raw materials $Ba(NO_3)_2$, $Sm(NO_3)_3.6H_2o$, & $Ce(NO_3)_3.6H_2o$ used starting materials including sodium carbonate Na_2CO_3 as precipitate agent. The stoichiometric molar ratios of $Ba_{0.2}Sm_{0.2}Ce_{0.6}O_{3-\delta}$ (Ba-SDC) were taken into account and their appropriate grams were obtained to start the synthesis process. In this context, the chemicals were measured with the help of weighing balance and 4.42 g of Samarium nitrate hex hydrate $Sm\ (NO_3)_3.\ 6H_2O$, 12.98 g Cerium nitrates hex hydrate $Ce\ (NO_3)_3.6H_2O$, and 2.6 g of Barium nitrate $Ba\ (NO_3)_2$ were measured. Samarium nitrate hex hydrate and Barium nitrate were introduced to the beakers along with 50 ml of deionized water and Cerium nitrates hex hydrate was introduced to the beakers along with 300 ml of deionized water. After magnetic bars were inserted in each beaker. Then these beakers were set on magnetic stirrers for 30 minutes to completely dissolve the nitrates.

After that to create a homogeneous solution, these three solutions were combined in a beaker of at least 500 ml and kept on a magnetic stirrer for one hour. After that, the precipitate agent of Na_2CO_3 with 1: 2 as BaSDC. Na_2CO_3 as 9.962 g dissolved deionized & solution obtained under the same circumstances. The obtained hot solution of Na_2CO_3 poured in the main solution under vigorous continuous stirring process at 500 rpm for two hours at 80℃. After that the solution were left alone 24 hours in tilted shape. The precipitates that formed were filtered by using vacuum filtration pump and washed three times with deionized water. These were dehydrated in a drying oven at 120℃ for 2 hours. After that a mortar pastel was used to grind the dry precipitates into a fine particles. The dried powder was then sintered in the crucible for 4 hours at 750℃. The nitrates were evaporated at temperatures between 250 and 300℃. Again the mortar and pestle were used to grind the resulting product into a fine powder.

This powder was then compressed into pellets by hydraulic press to determine the conductivity of the resulting material.

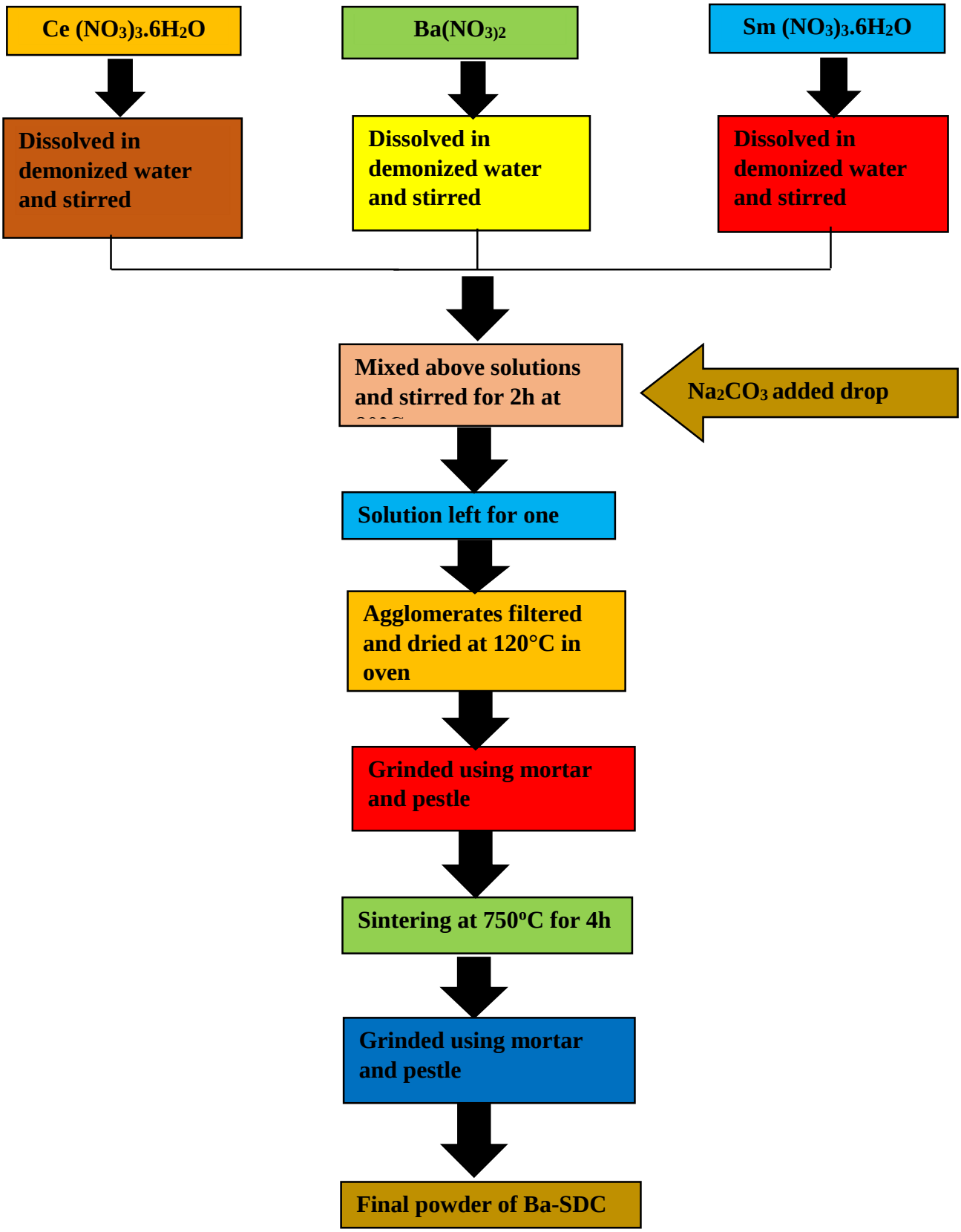

Figure 3. 2 Synthesis of Ba-SDC

3.7 Experimental procedure for Sr-SDC

Strontium, Samarium co-doped Cerium Oxide electrolyte material for SOFC was successfully synthesized by co-precipitation method. The following raw materials $Sr(NO_3)_3$, $Sm(NO_3)_3.6H_2o$, and $Ce(NO_3)_3.6H_2o$ used starting materials including sodium carbonate Na_2CO_3 as precipitate agent. The stoichiometric molar ratios of $Sr_{0.2}Sm_{0.2}Ce_{0.6}O_{3-\delta}$ (SrSDC) were taken into account and their appropriate grams were obtained to start the synthesis process. In this context, the chemicals were measured with the help of weighing balance and 4.54 g of Samarium nitrate hex hydrate $Sm\ (NO_3)_3.\ 6H_2O$, 13.3 g of Cerium nitrates hex hydrate $Ce\ (NO_3)_3.6H_2O$, and 2.16 g of Strontium nitrate $Sr\ (NO_3)_3$ were measured. Samarium nitrate hex hydrate and Strontium nitrate were introduced to the beakers along with 50 ml of deionized water and Cerium nitrates hex hydrate was introduced to the beakers along with 300 ml of deionized water. After magnetic bars were inserted in each beaker. Then these beakers were set on magnetic stirrers for 30 minutes to completely dissolve the nitrates.

After that to create a homogeneous solution, these three solutions were combined in a beaker of at least 500 ml and kept on a magnetic stirrer for one hour. After that, the precipitate agent of Na_2CO_3 with 1: 2 as SrSDC. Na_2CO_3 as 10.599 g was dissolved into deionized water and the solution was obtained under the same circumstances. The obtained hot solution of Na_2CO_3 was poured into the main solution under vigorous continuous stirring process at 500 rpm for two hours at 80℃. After that the solution were left alone 24 hours in tilted shape. The precipitates that formed were filtered by vacuum filtration pump & washed three times with deionized water. These were dehydrated in a drying oven at 120℃ for 2 hours. After that a mortar pastel was used to grind the dry precipitates into a fine particles. The dried powder was then sintered in the crucible for 4 hours at 750℃. The nitrates were evaporated at temperatures between 250 and 300℃. Again the mortar and pestle were used to grind the resulting product into a fine powder.

This powder was then compressed into pellets by hydraulic press to determine the conductivity of the resulting material.

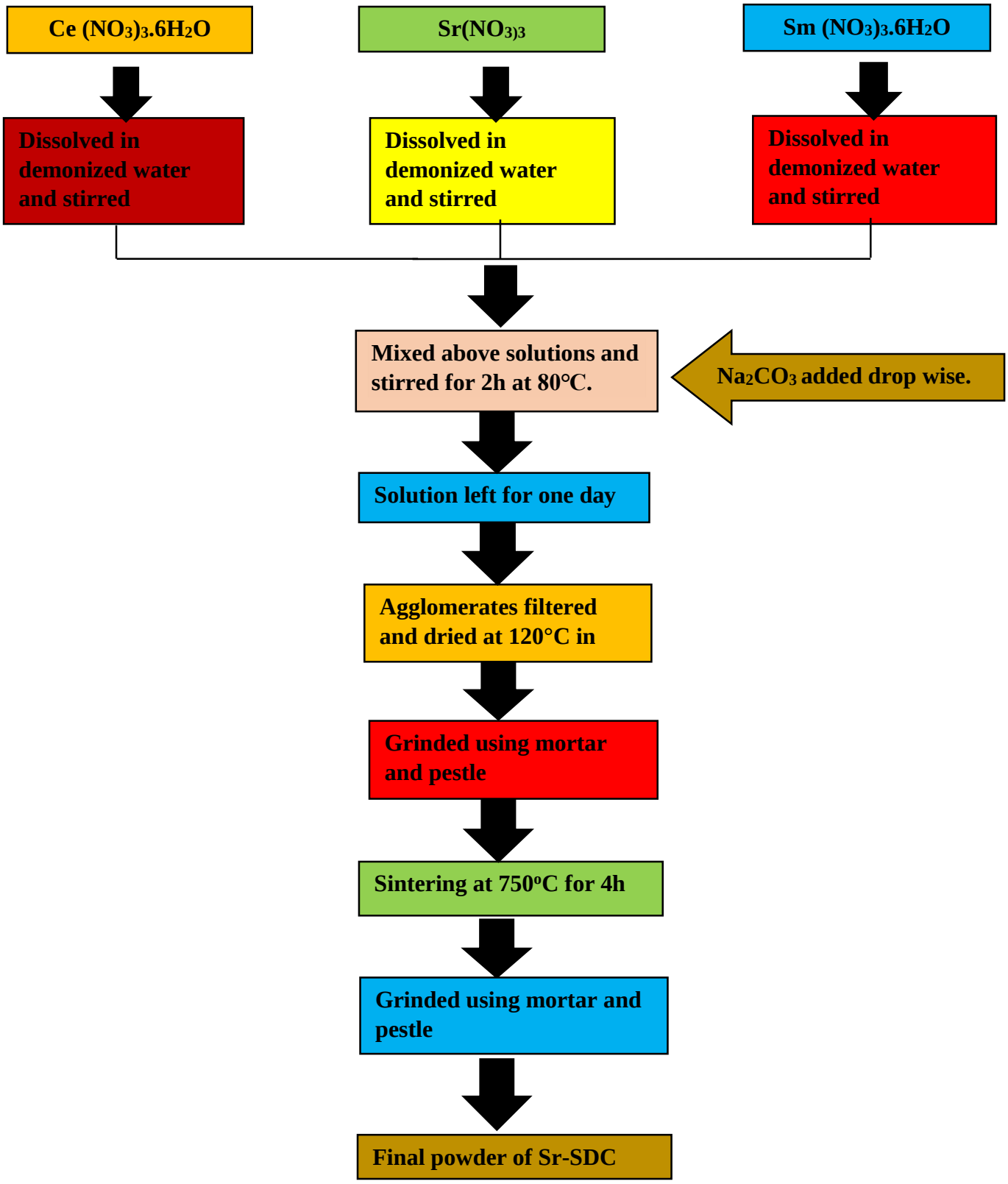

Figure 3. 3 synthesis of Sr-SDC powder

3.8 Experimental procedure for Ca-SDC

Calcium, Samarium co-doped Cerium Oxide electrolyte material for solid oxide fuel cell was successfully synthesized by co-precipitation method. The following raw materials $Ca(NO_3)_3.4H_2O$, $Sm(NO_3)_3.6H_2o$, and $Ce(NO_3)_3.6H_2o$ were used as starting materials including sodium carbonate Na_2CO_3 as precipitate agent. stoichiometric molar ratios $Ca_{0.2}Sm_{0.2}Ce_{0.6}O_{3-\delta}$ (CaSDC) were taken into account and their appropriate grams were obtained to start the synthesis process. In this context, the chemicals were measured with the help of weighing balance and 4.48 g of $Sm(NO_3)_3.6H_2O$, 13.14 g of Cerium nitrates hexahydrate $Ce(NO_3)_3.6H_2O$, and 2.38 g of Calcium nitrate tetrahydrate $Ca(NO_3)_3.4H_2O$ were measured. Samarium nitrate hexahydrate and Calcium nitrate tetrahydrate were introduced to the beakers along with 50 ml of deionized water and Cerium nitrates hexahydrate was introduced to the beakers along with 300 ml of deionized water. After magnetic bars were inserted in each beaker. Then these beakers were set on magnetic stirrers for 30 minutes to completely dissolve the nitrates.

After that to create a homogeneous solution, these three solutions were combined in a beaker of at least 500 ml and kept on a magnetic stirrer for one hour. After that, the precipitate agent of Na_2CO_3 with 1: 2 as CaSDC. Na_2CO_3 as 10.599 g dissolved into deionized water & the solution was obtained under the same circumstances. The obtained hot solution of Na_2CO_3 was poured into the main solution under vigorous continuous stirring process at 500 rpm for two hours at 80℃. After that the solution were left alone 24 hours in tilted shape. The precipitates that formed were filtered by using vacuum filtration pump & washed three times with deionized water. These were dehydrated in a drying oven at 120℃ for 2 hours. After that a mortar pastel was used to grind the dry precipitates into a fine particles. The dried powder was then sintered in the crucible for 4 hours at 750℃. The nitrates were evaporated at temperatures between 250 and 300℃. Again the mortar and pestle were used to grind the resulting product into a fine powder.

This powder was then compressed into pellets by hydraulic press to determine the conductivity of the resulting material.

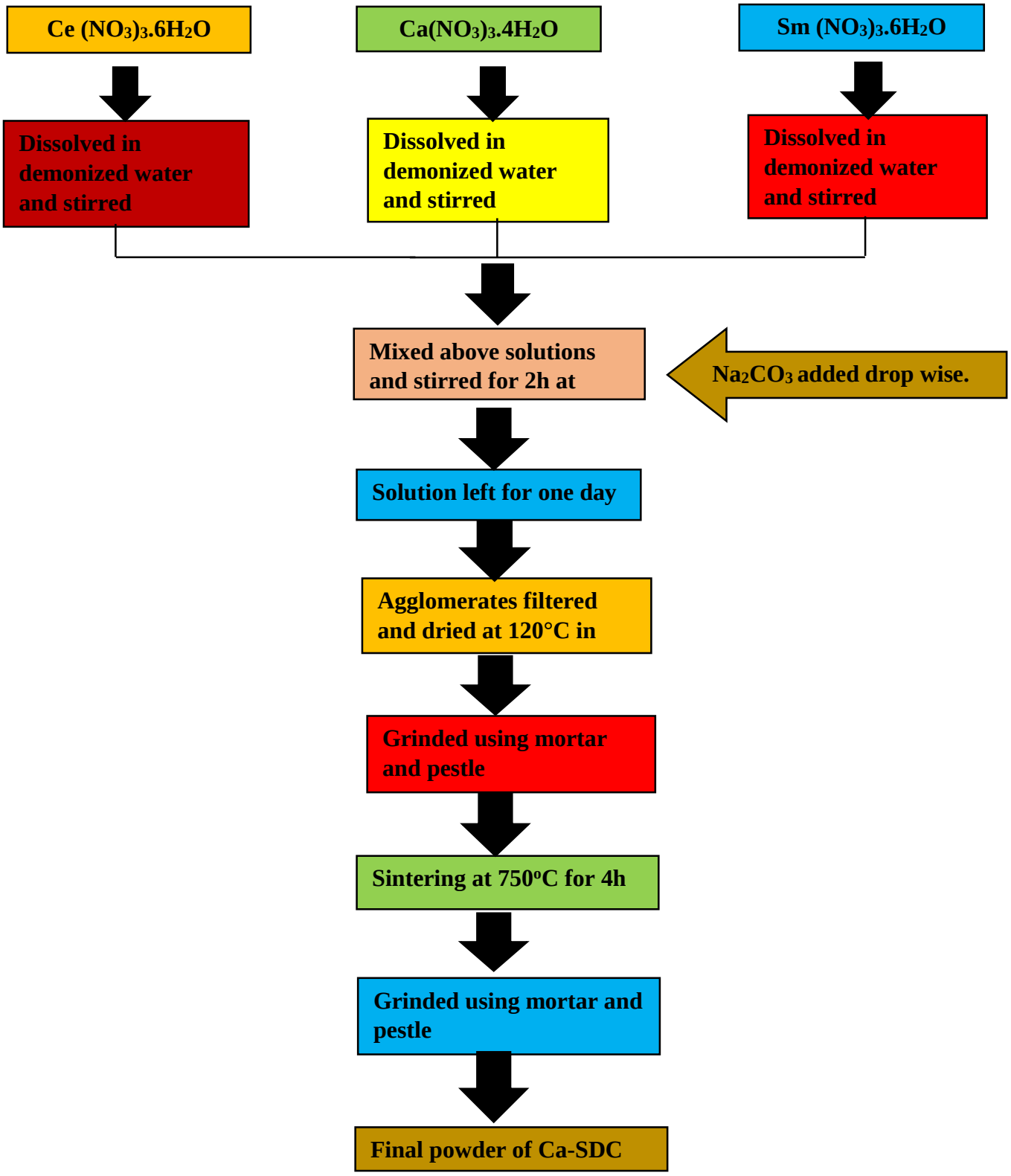

Figure 3. 4 synthesis of Ca-SDC powder

3.9 Experimental procedure for Ti-SDC

Titanium, Samarium co-doped Cerium Oxide electrolyte material SOFC was successfully synthesized by co-precipitation method. The following raw materials TiO_2, $Sm(NO_3)_3.6H_2o$, and $Ce(NO_3)_3.6H_2o$ were used as starting materials including sodium carbonate Na_2CO_3 as precipitate agent. The stoichiometric molar ratios of $Ti_{0.2}Sm_{0.2}Ce_{0.6}O_{3-\delta}$ (TiSDC) were taken into account and their appropriate grams were obtained to start the synthesis process. In this context, the chemicals were measured with the help of weighing balance and 4.86 g of $Sm\ (NO_3)_3.\ 6H_2O$, 14.26 g of Cerium nitrates hexahydrate $Ce\ (NO_3)_3.6H_2O$, 0.88 g Titanium dioxide TiO_2 were measured. Samarium nitrate hexahydrate introduced to the beakers along with 50 ml of deionized water. Titanium dioxide wasn't dissolved in deionized water directly so, first Titanium dioxide was dissolved in 18ml of sulphric acid and then introduced to the beaker along with 50 ml of deionized water. After Cerium nitrates hexahydrate was introduced to the beakers along with 300 ml of deionized water. After magnetic bars were inserted in each beaker. Then these beakers were set on magnetic stirrers for 30 minutes to completely dissolve the nitrates.

After that to create a homogeneous solution, these three solutions were combined in a beaker of at least 500 ml and kept on a magnetic stirrer for one hour. After that, the precipitate agent of Na_2CO_3 with 1: 2 as TiSDC. Na_2CO_3 as 11.659 g was dissolved into deionized water and the solution was obtained under the same circumstances. The obtained hot solution of Na_2CO_3 was poured into the main solution under vigorous continuous stirring process at 500 rpm for two hours at 80℃. After that the solution were left alone 24 hours in tilted shape. The precipitates that formed were filtered by using vacuum filtration pump and washed three times with deionized water. These were dehydrated in a drying oven at 120℃ for 2 hours. After that a mortar pastel was used to grind the dry precipitates into a fine particles. The dried powder was then sintered in the crucible for 4 hours at 750℃. The nitrates were evaporated at temperatures between 250 and 300℃. Again the mortar and pestle were used to grind the resulting product into a fine powder.

This powder was then compressed into pellets by hydraulic press to determine the conductivity of the resulting material.

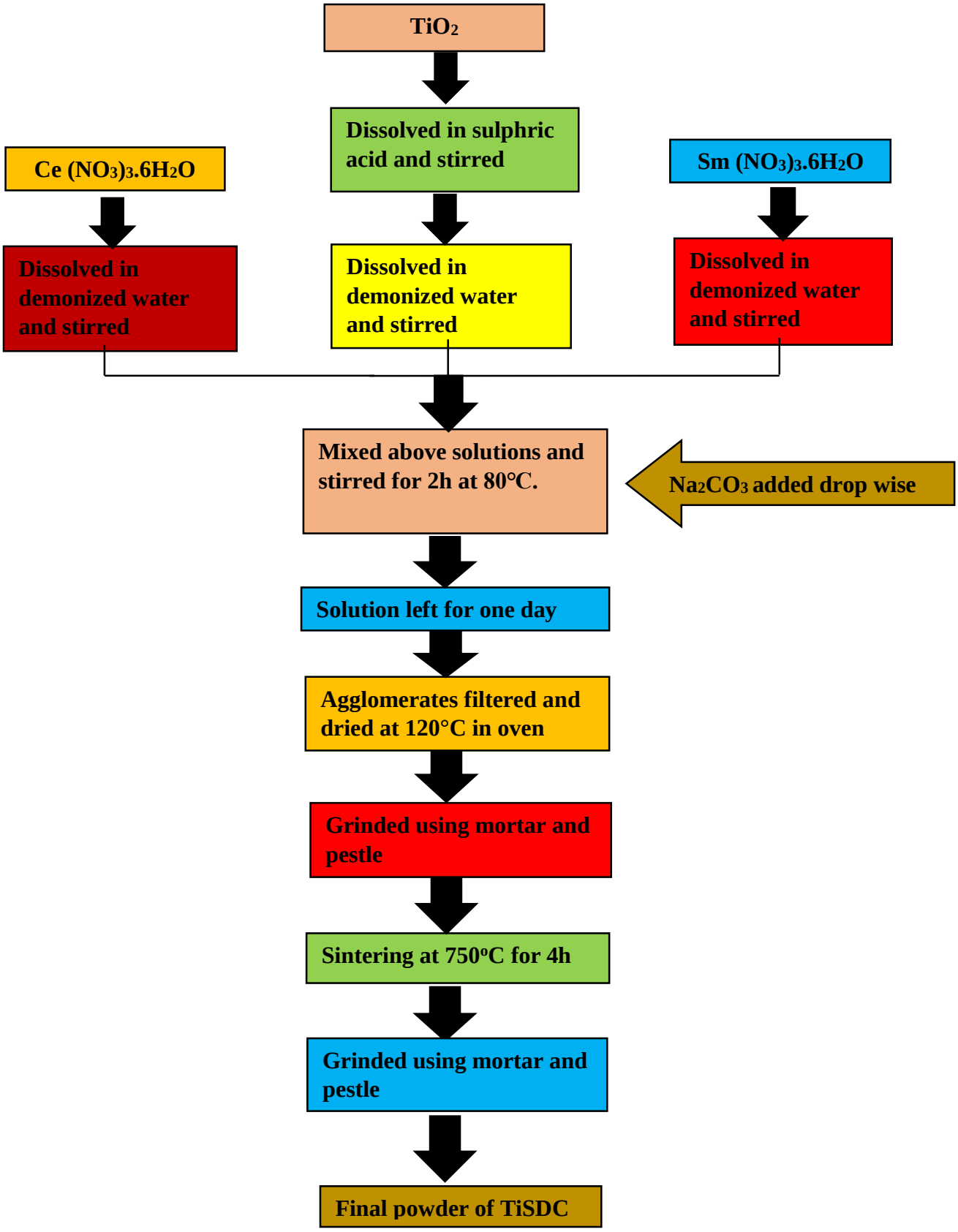

Figure 3. 5 synthesis of Ti-SDC powder

3.10 Cell fabrication

Appropriately 0.8–1g of powder were collected and pressed into a cell using a Crave hydraulic press. Dry powder is used in the method. To construct a complete cell, the powder is loaded into stainless steel and then pressed in one motion at a tension of 3000 MPa as shown in Figure 3.6

Carver hydraulic press Cell without sliver paste Cell with sliver paste

Figure 3. 6 Cell fabrication method

There were 13 mm of total cell width and 0.64 cm^2 of active area. These cells were sintered for 30 minutes at 600 degrees to produce dense cells. Sliver paint has been sprayed on both sides of the cell in the present collection, as seen in the top figure. To measure conductivity, the prepared cell was used. For a fuel cell to function, an electrolyte sandwiched between the anode and cathode is used.

3.11 Characterization Techniques

The various properties of the newly synthesized material are evaluated using a variety of characterization techniques after electrolyte manufacturing. The investigation of phase formation and doping using Raman spectroscopy. The band gap of a substance can be found using UV-V spectroscopy. Utilizing FTIR, the bond formation was examined. Using EIS, conductivity of the material was measured. In this section, we'll briefly go through each of these tactics.

¶ Raman spectroscopy

¶ UV-Vis Spectroscopy

¶ Fourier Transmission Infrared spectroscopy (FTIR)

¶ Conductivity Measurement

¶ Fuel Cell Performance

3.11.1 Raman Spectroscopy

This technique locates a substance's vibrational energy modes by using dispersed light. Raman spectroscopy frequently yields a structural fingerprint that can be used to identify substances. Examining molecular vibrations, crystal structure, inorganic materials, and foreign material particles smaller than one micron can all be done with Raman spectroscopy, while FTIR cannot.

Elastic or inelastic scattering of light is possible when it interacts. The term Rayleigh scattering is used to describe elastic scattering. It in this context is irrelevant and offers no useful information. In contrast to in elastically scattered light, Ra-man scattering provides knowledge about and changes rotational, electron & vibrational energy of molecule. It is made up of the inelastic scattering of monochromatic ultraviolet light. When laser interacts with phonons, the energy of laser photons is altered upward or downward. For illuminating a sample, a laser beam is commonly employed. When an incident source interacts with a sample, its energy changes, causing what is known as a Raman shift. As a general rule, Raman spectroscopy is a fingerprint technique that is utilized for a particular material and quickly determines the nature and behavior of materials while also separating it from other materials [50].

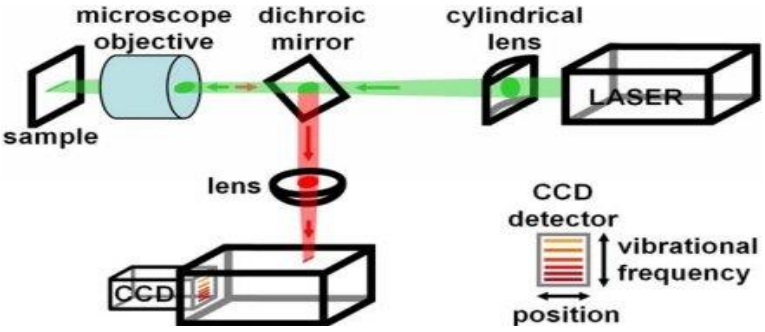

Figure 3. 7 Schematic diagram of Raman Spectra

3.11.2 UV-Vis Spectroscopy

To analyze a variety chemicals, UV-VISIBLE spectroscopy is a common spectrophotometric technique. A sample's light absorption is revealed via UV spectroscopy methods. According to the manner in which chemical molecules absorb visible or ultraviolet light to create unique spectrum, UV-Visible Spectroscopy can be used to study a variety of different materials.

It is sufficient to measure how much radiation enters the sample. With the help of UV light absorption, electrons can transition from one excited state to another, releasing energy. Only by the use of low-energy electrons can organic materials absorb UV and visible light. The molecule's electronic energy changes as a result of UV light. One electron is moved from a molecular orbital that is occupied and has a low potential energy to an unfilled molecular orbital with a higher potential energy as the molecule gains energy. This characterization process can be used to identify the energy band gap and UV-VIS spectra of the produced material [51].

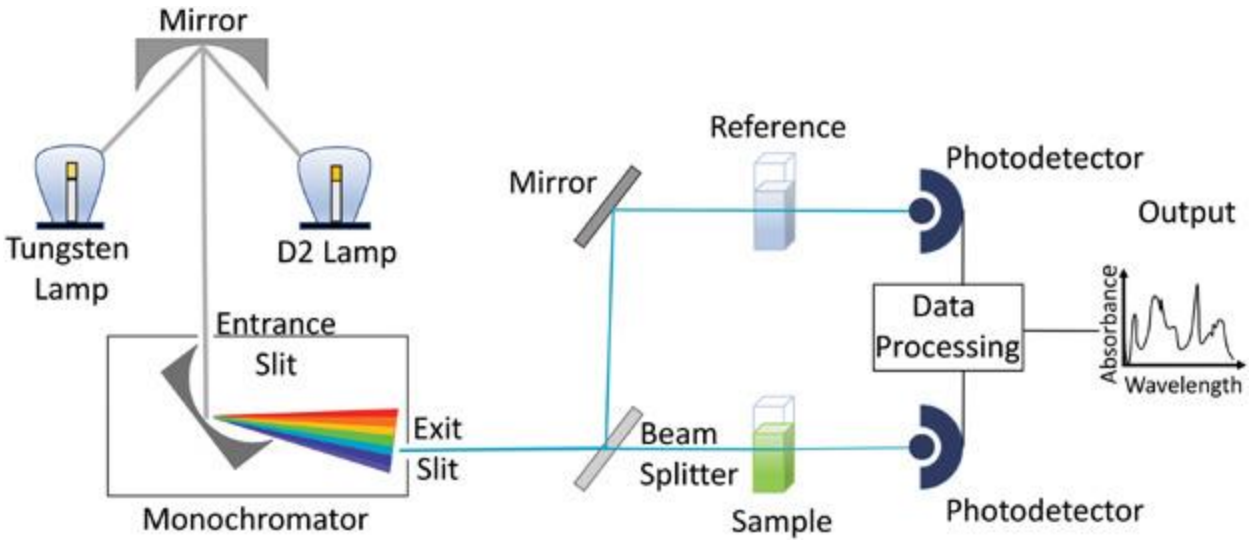

Figure 3. 8 Schematic diagram of UV-Visible Spectra

3.11.3 FTIR spectroscopy

Fourier transformation infrared spectroscopy is used to assess molecular and functional groups of substance. It discloses the presence of organic and inorganic components in the sample. Additionally, it tells you whether a particular item may contain contaminants. The FTIR spectrometer gathers high-resolution data at a variety of wavelengths. FTIR is a method for figuring out how the intensity of infrared light changes when it interacts with a material. Over a wide range of wave numbers, it can identify chemical bonds in a material. A spectrum is constructed based on the chemical bonds found in each sample when an infrared beam interacts with it, using the data for transmittance or absorbance. A change in the interatomic spacing along the bond axis is referred to as stretching. Peaks of absorption during stretching are higher than those during bending. Change in angle between two bonds is referred as bending. In the majority of FTIR analyses, we observe data in three components. Peak position comes first, then peak width, and then peak intensity. Because each molecule has a unique peak position, we can identify which one it is. Peak width indicates the type of functional group that bonds to the molecule, whereas peak intensity indicates the vibrational energy of the molecule [52].

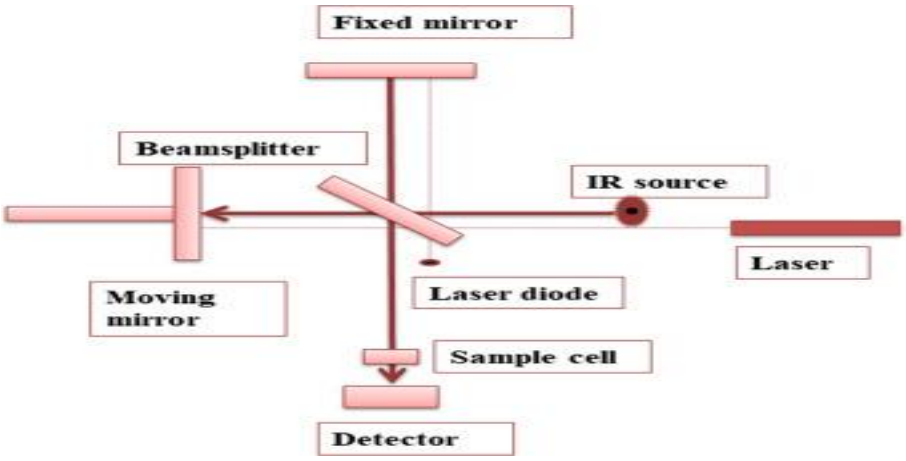

Figure 3. 9 Schematic diagram of FTIR Spectra

3.11.4 Conductivity Measurement

Electrochemical Impedance Spectroscopy (EIS) & DC four point probe technique are typically used to calculate conductivity of materials, because its yield is more accurate findings, the EIS technique is utilized to assess conductivity. The conductivity (Scm^{-1}) is calculated by following formula:

$$б = L / RA$$

- L= Thickness of cell
- R= Resistance of materials
- A= Area of cell

3.11.5 Fuel cell performance

A test holder with cathode, electrolyte, and anode used to evaluate the electrochemical fuel cell performance of manufactured material. Test holder was inserted into the electrically heated furnace. The anode gets hydrogen fuel, and the air pump machine supplies the cathode with oxygen. Silver coatings are applied to the cathode and anode sides to deal with low resistance and high current. Between 500 and 700 °C is expected to be the optimal operating temperature range for electrochemical fuel cells. The voltage, current, and open circuit voltage were measured when a load was applied using a fuel cell performance testing instrument.

Fuel cell test holder

Fuel cell testing set-up

Figure 3. 10 Schematic diagram of Fuel cell testing

Chapter 4

Results & Discussion

4.1 Raman Spectroscopy

The processed materials' Raman spectra were collected in order to learn important information regarding their bonding, vibrational modes, structure, and chemical composition. Materials (Ba-SDC, Sr-SDC, Ca-SDC and Ti-SDC) sintered at 750 °C had their Raman spectra captured using by RENISHAW UK's In Via Raman microscope with a laser wavelength of 514 nm in range of 100-1400/cm wave numbers [53].

The Raman spectra of the materials (Ba-SDC, Sr-SDC, Ca-SDC, Sr-SDC and Ti-SDC) individually displays the spectrum at 750°C. The strongest peak of BaO located at 1056 $cm^{-1}$and CeO_2 at 461 cm^{-1} represented F_{1g} mode as shown in Figure 4.1.

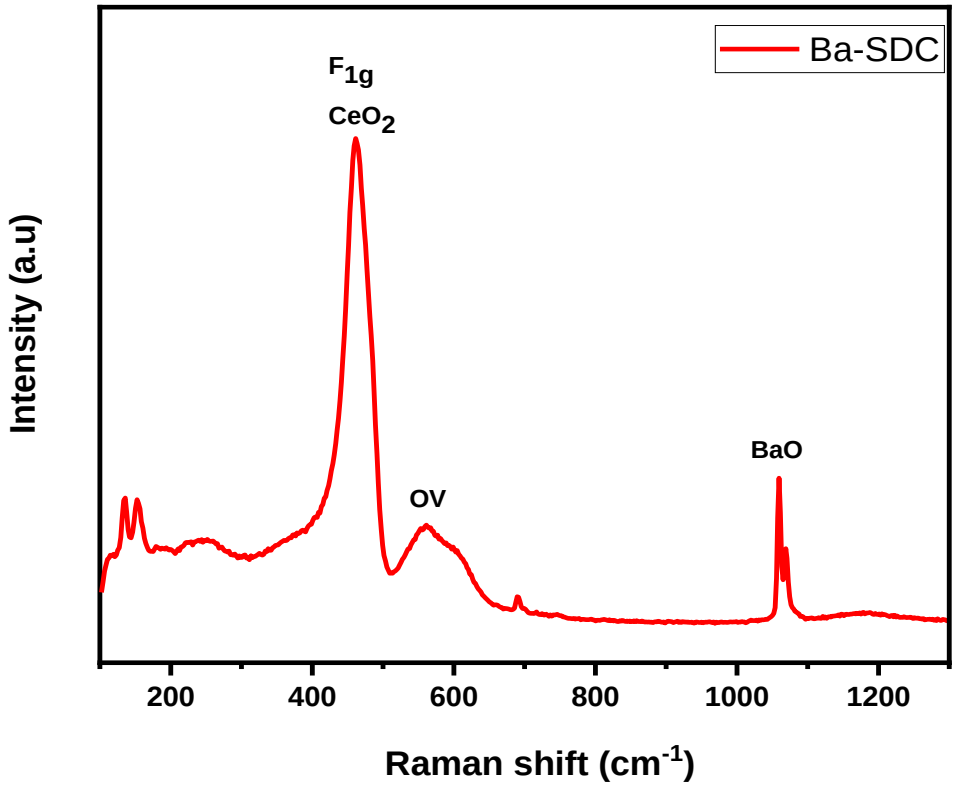

Figure 4. 1 Raman spectra of Ba-SDC

Strongest peak of SrO, located at 1070 cm^{-1} represented A_{1g} mode and CeO_2 located 463 cm^{-1} represented F_{1g} mode as shown in Figure 4.2

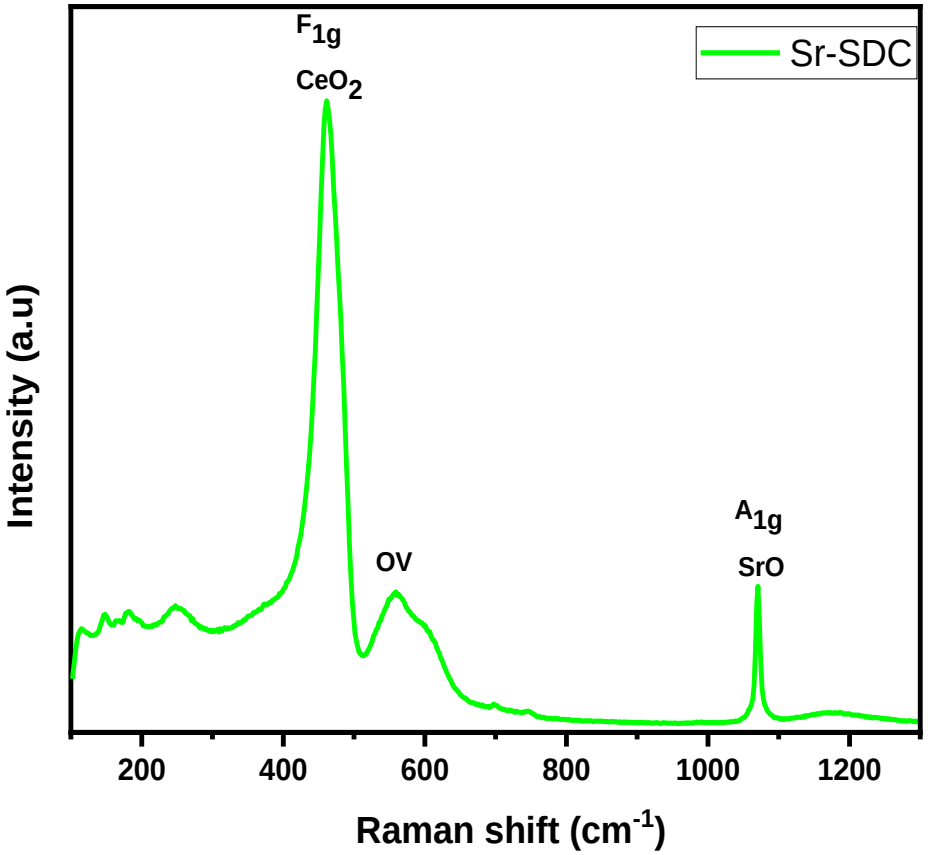

Figure 4. 2 Raman spectra of Sr-SDC

Strongest peak of CaO, located at 114 cm^{-1}, 1085 cm^{-1} and CeO_2 located 463 cm^{-1} represented F_{1g} mode as shown in Figure 4.3.

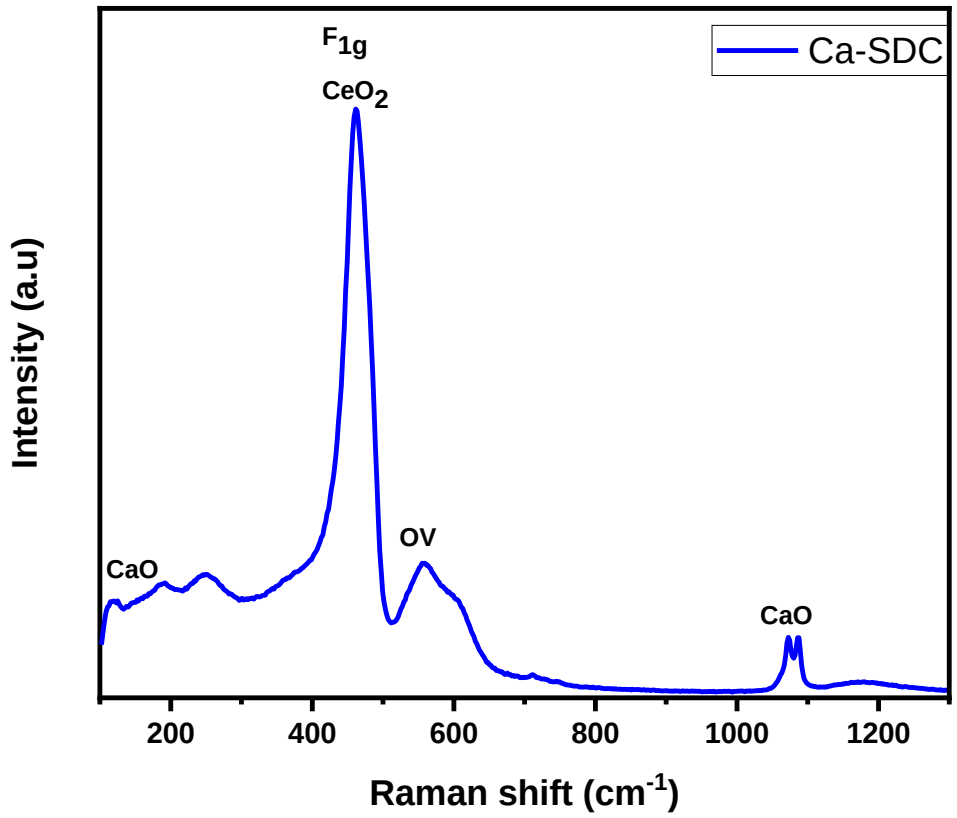

Figure 4. 3 Raman spectra of Ca-SDC

Strongest peak of TiO_2 located at 139 cm^{-1}, 636 cm^{-1} represented E_g mode ,CeO_2 located 461 cm^{-1} represented F_{1g} mode and H_2SO_4 located at 991 cm^{-1} 1027 cm^{-1} as shown in Figure 4.4.

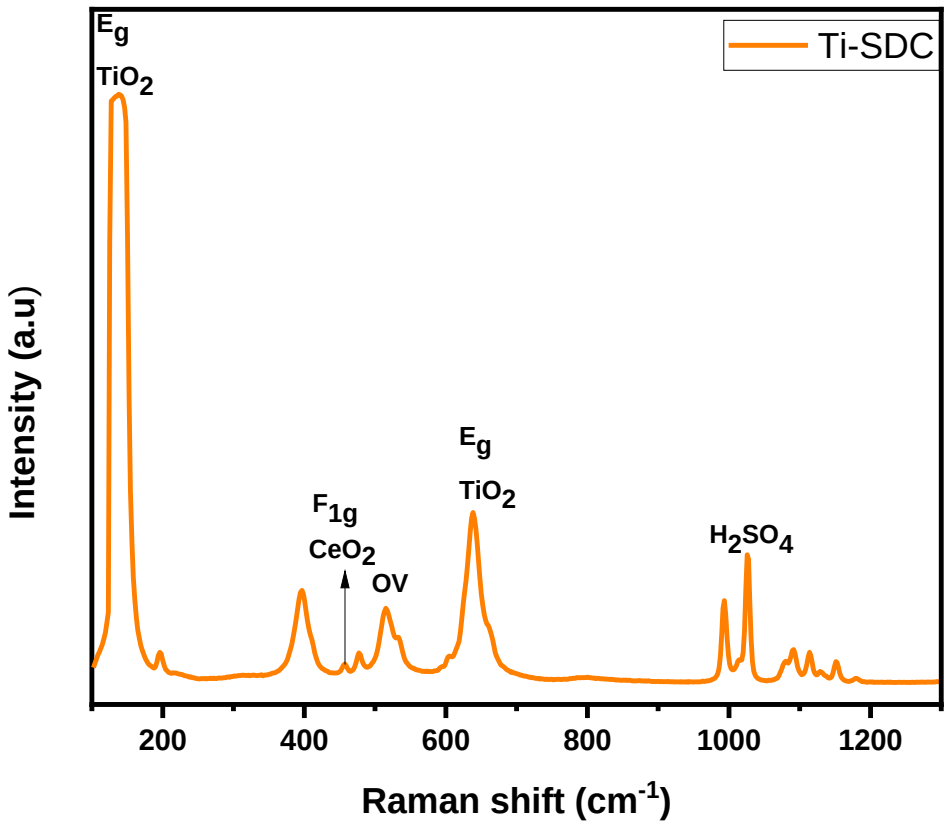

Figure 4. 4 Raman spectra of Ti-SDC

Figure 4.5 show combined Raman spectra of materials (Ba-SDC, Sr-SDC, Ca-SDC, Sr-SDC and Ti-SDC)

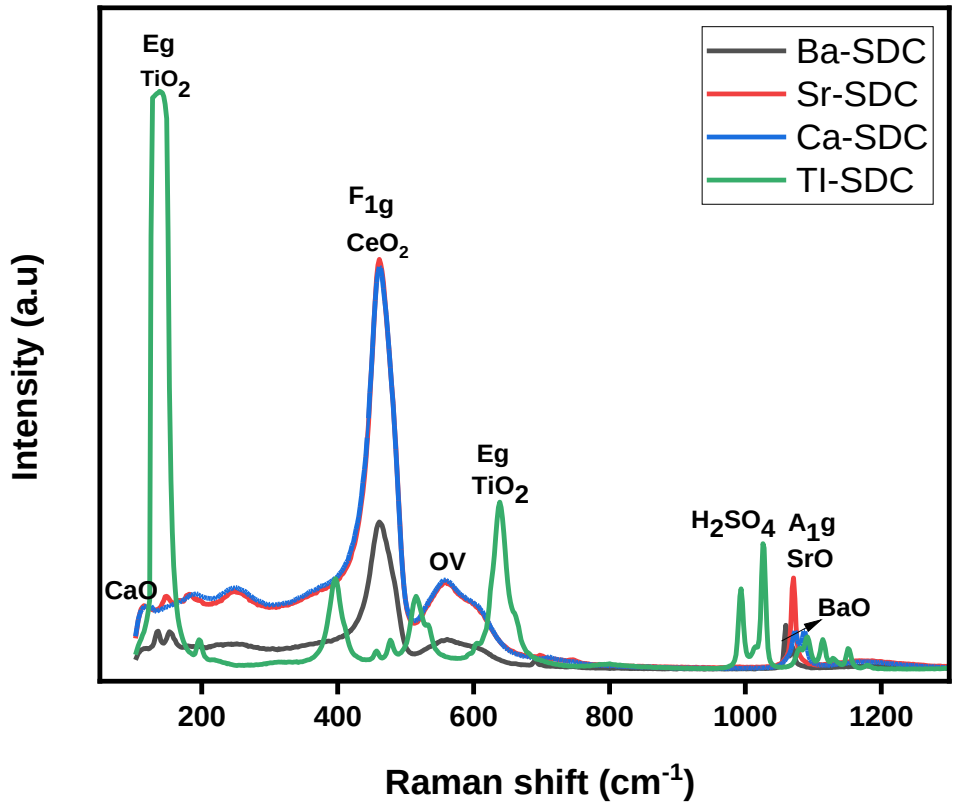

Figure 4. 5 Combined Raman spectra of (Ba-SDC, Sr-SDC, Ca-SDC and Ti-SDC)

The primary peaks in the spectrum are identified as CeO_2, BaO, CaO, SrO, TiO_2, H_2SO_4 and OV (oxide vacancies), respectively, situated at 463 cm^{-1}, 1061 cm-^{1}, 1088cm^{-1}, 1070 cm^{-1}, 139 cm^{-1}, 991 cm^{-1} and 555 cm^{-1}[54-60]. The Raman spectra of CeO_2 nanoparticles has first order Raman peak (F_{1g}) at 463 cm^{-1} based on the size of the crystallites. Due to the effect of size, Raman mode at 463 cm^{-1} is susceptible to alterations in the oxygen stoichiometry of CeO_2. The O-O bonds in the strontium oxide lattice are symmetrically stretched. causes the most intense peak to appear at about 1070 cm^{-1}. The A_{1g} peak is the more frequent name for this peak. The produced TiO_2-NPs' Raman spectra shows a strong Eg mode at 139 cm^{-1}. The bending, asymmetric, and symmetric vibrations of the Ti–O–Ti link are the cause of the vibrational modes. Raman spectra the blue shift is created when the wavelength is decrease and wave number increase. If the blue shift happens, the particle

size dimension will also expand and the energy band gap will widen as well as red shift is created when wave length increase, wave number decrease. If red shift happen means particle size dimension will also decrease and the energy band gap will narrowing.

4.2 UV- Visible Analysis

To observe the strong band gap (Eg) and band shape, one tool is to study UV-visible spectra. Through the use of UV-visible spectra, the energy band gap and absorbance for the synthesized sample are detected.

Tauc's equation was used to compute the electrolyte material's ban gap.

$$(\alpha h\nu)^n = A(h\nu - E_g)$$

E_g is energy band gap

α is absorption coefficient

h is Planks constant

A is constant

n is to determine the band gap

The value of power ‘n’ decides whether band gap is direct or indirect. If value of n is half means indirect band gap and if value of n is 2 means direct band gap. Figure 4.6 display the energy band gap of Ba-SDC material with the help of Tauc equation, detect band gap is calculated which is 3.89eV. Maximum peak is determined at 210, 245,260 and 270 which is in UV-visible area.

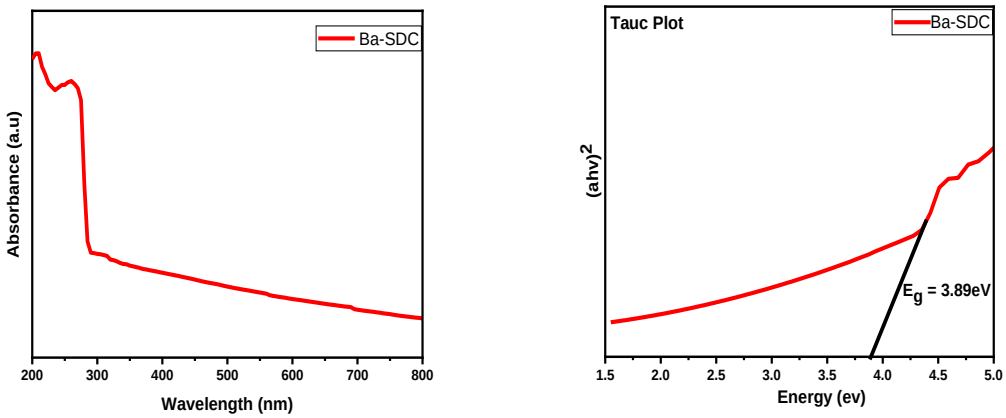

Figure 4. 6 UV-Visible spectra of Ba-SDC

Figure 4.7 display the energy band gap of Sr-SDC material with the help of Tauc equation, detect band gap is calculated which is 3.72eV. Maximum peak is determined at 210 and 245 which is in UV-visible area.

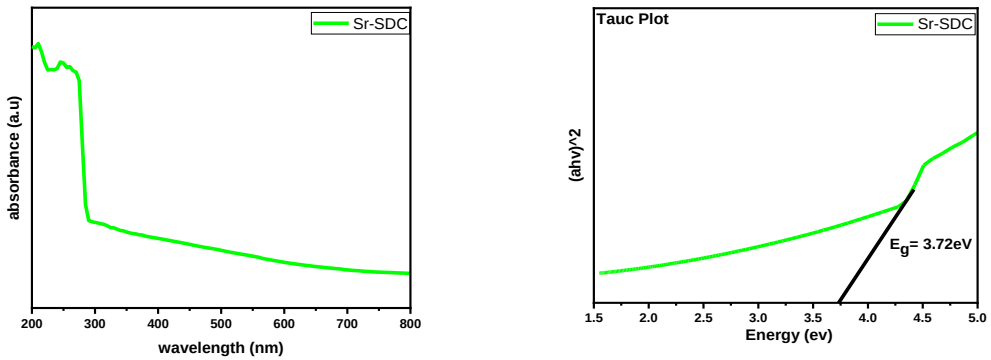

Figure 4. 7 UV-Visible spectra of Sr-SDC

Figure 4.8 display the energy band gap of Ca-SDC material with the help of Tauc equation, detect band gap is calculated which is 3.72eV. Maximum peak is determined at 205,245 and 270 which is in UV-visible area.

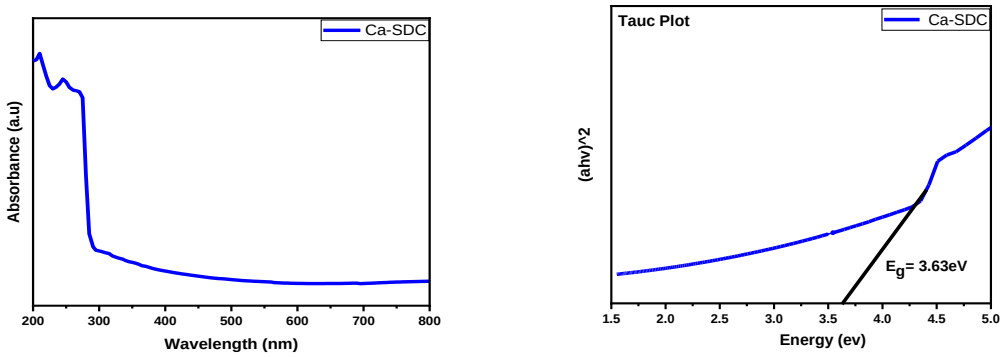

Figure 4. 8 UV-Visible spectra of Ca-SDC

Figure 4.9 display the energy band gap of Ca-SDC material with the help of Tauc equation, detect band gap is calculated which is 3.68eV. Maximum peak is determined at 210,245 and 270 which is in UV-visible area.

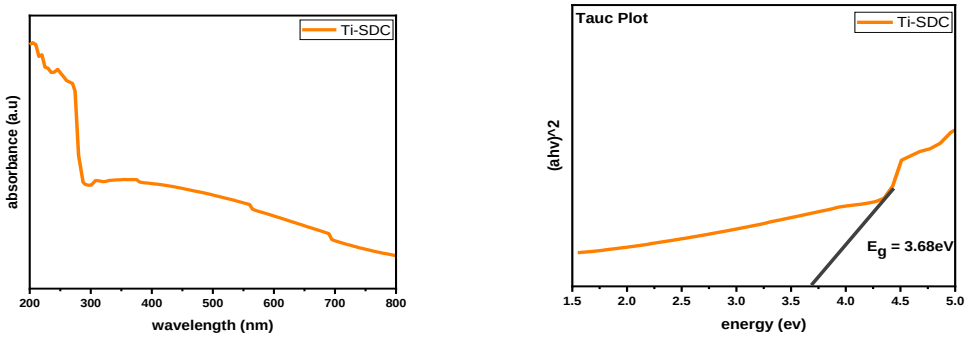

Figure 4. 9 UV-Visible spectra of Ti-SDC

4.3 FTIR spectroscopy

This is one of the most significant techniques since it simultaneously measures intensity throughout wavelength and provides information about imaginary groupings. Information on the emission and absorption spectra of solids, liquids, and gases can also be obtained by FTIR spectroscopy. Basically in FTIR, there are two regions: functional region and fingerprint region. Fingerprint region vibrations occur at 500-1500cm^{-1}. Where in

functional group region vibrations (double bound like C=O, C=C, C=N) occur at 1500-2000cm^{-1}. Triple bound vibrations occur at 2000-2500cm^{-1}. Single bound stretch like O-H, N-H, C-H occur at 2500-4000cm^{-1}. In my samples SDC is common. The Ce-O vibrations in the SDC sample give rise to the band near 675 cm^{-1}. Band near at 1033 cm^{-1} corresponds to Sm-O bond [61].

FTIR analysis of Ba-SDC

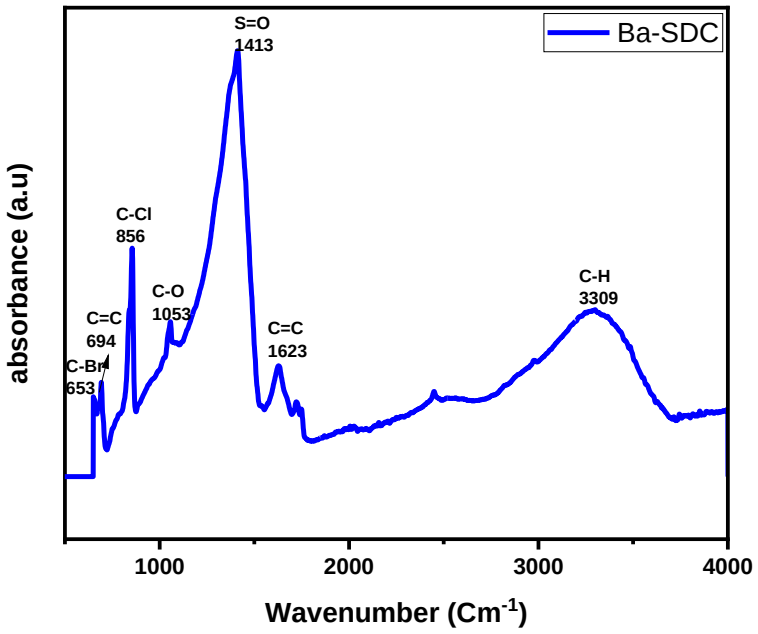

Figure 4. 10 FTIR spectra of Ba-SDC

The FTIR spectra of the Ba-SDC shown in Figure 4.10. The broad band centered 3309 cm^{-1} due to C-H stretching. Band at 1623 cm^{-1} are mainly by C=C group stretching vibration. Band near 1413 cm^{-1} due to S=O stretching mode & band near 1053 cm^{-1} is due to C-O stretching mode. The band near 694cm^{-1} is due to C=C bending mode and the band centered at 653 cm^{-1} due to C-Br stretching mode.

FTIR analysis of Sr-SDC

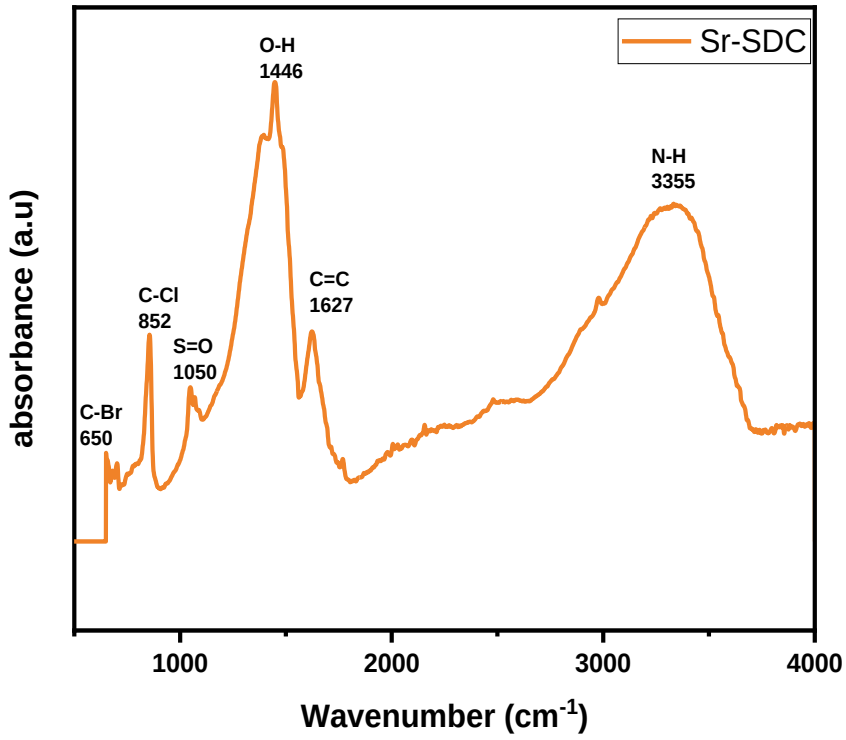

Figure 4. 11 FTIR spectra of Sr-SDC

The FTIR spectra of the Sr-SDC are shown in Figure 4.11. The broad band centered at 3355 cm^{-1} is due to N-H stretching. band at 1627 cm^{-1} are mainly due to the C=C group stretching vibration. The band near 1446 cm^{-1} is due to O-H bending mode & band near 1050 cm^{-1} is due to S=O stretching mode. The band near 852cm^{-1} is due to C-Cl stretching mode and the band centered at 650 cm^{-1} due to C-Br stretching mode.

FTIR analysis of Ca-SDC

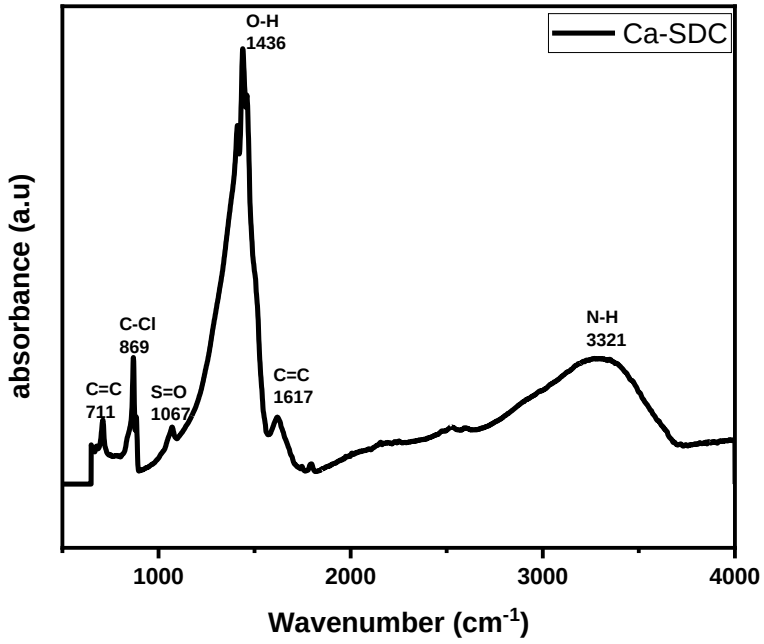

Figure 4. 12 FTIR spectra of Ca-SDC

FTIR spectra of Ca-SDC are shown in Figure 4.12. Broad band centered at 3321 cm^{-1} is due to N-H stretching. The band at 1617 cm^{-1} are mainly due to the C=C group stretching vibration. The band near 1436 cm^{-1} is due to O-H bending mode. A band near 1067 cm^{-1} is due to S=O stretching mode. The band near 869cm^{-1} is due to C-Cl stretching mode and the band centered 711 cm^{-1} due to C=C bending mode.

FTIR analysis of Ti-SDC

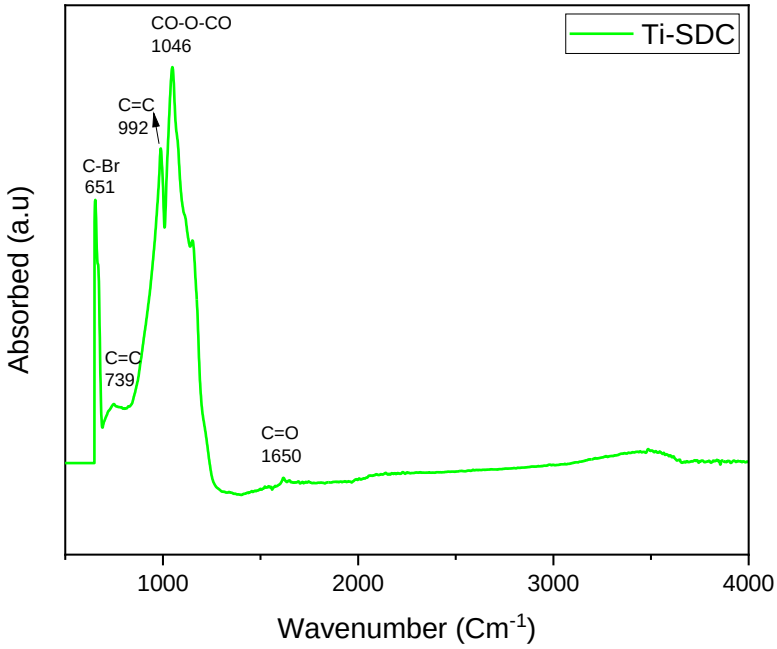

Figure 4. 13 FTIR spectra of Ti-SDC

The FTIR spectra of the Ti-SDC are shown in Figure 4.13. The band centered at 1650 cm^{-1} is due to C=O stretching. Band at 1046 cm^{-1} are mainly due to the CO-O-CO group stretching & vibration. Band near 992 cm^{-1} is due to C=C bending mode. The band near 739 cm^{-1} is also due to C=C bending mode. Band centered at 651 cm^{-1} due to C-Br stretching mode.

4.4 Conductivity of Material (Ba-SDC, Sr-SDC, Ca-SDC &Ti-SDC)

In order to get high performance SOFC, conductivity is crucial. It is measured by EIS using various temperatures, such as 500°C, 600°C, and 700°C. In measuring conductivity, temperature is crucial. Conductivity rises when ion mobility rises. The below graph displays the conductivity of different materials as determined using EIS. The graph illustrates the relationship between temperature and conductivity and also demonstrates how ionic conductivity increases with temperature. Temperature increases also cause an increase in oxygen vacancies, which increases material conductivity. At 700°C, the maximum value of the material Ti-SDC is 0.090 S/cm. The indicated ionic conductivity was caused by smaller crystalline size, greater density values, and the mobility of dopant ions [62].

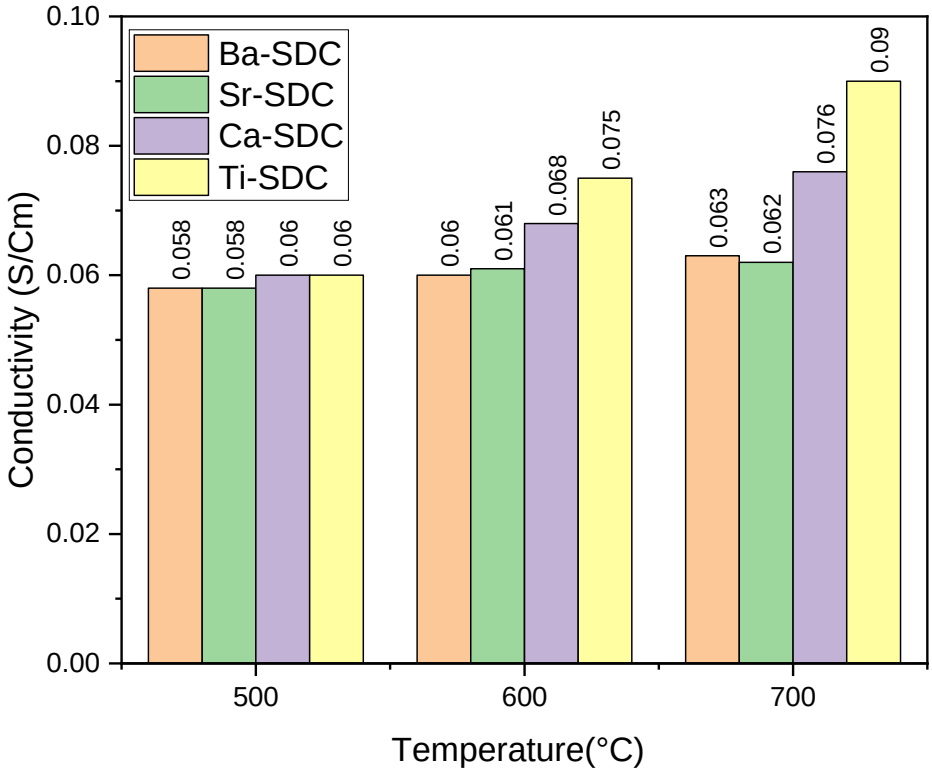

Figure 4. 14 Conductivity measurement of material (Ba-SDC, Sr-SDC, Ca-SDC and Ti-SDC

Materials	Temperature (°C)			Resistance (Ω)			Conductivity (S/cm)		
Ba-SDC	500	600	700	0.46	0.48	0.50	0.058	0.060	0.063
Sr-SDC	500	600	700	0.46	0.49	0.50	0.058	0.061	0.062
Ca-SDC	500	600	700	0.48	0.54	0.61	0.060	0.068	0.076
Ti-SDC	500	600	700	0.48	0.60	0.72	0.060	0.075	0.090

Table 4. 1 Temperature vs Conductivity

4.5 Fuel Cell Performance

The constructed cell's performance was evaluated at 500°C, 600°C & 700°C temperature using hydrogen gas as the fuel. The three layers of the prepared cell, which included the prepared electrolyte material and LNCZ-used as anode and cathode. The graph between open circuit voltage (OCV) and temperature.

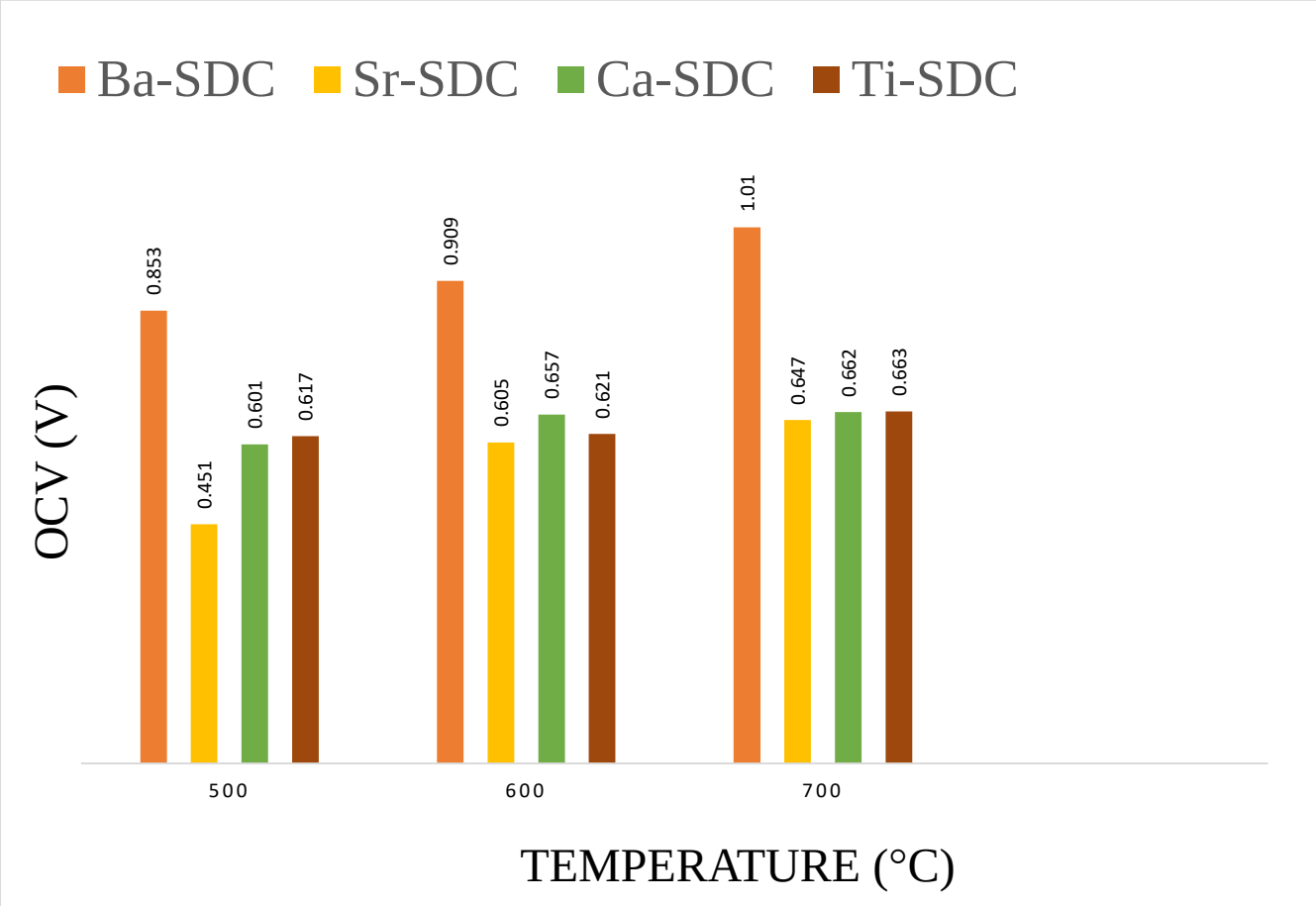

Figure 4. 15 Fuel cell performance of material (Ba-SDC, Sr-SDC, Ca-SDC and Ti-SDC)

Conclusion

The co-precipitate method was used in this study to manufacture the electrolyte materials (Ba-SDC, Sr-SDC, Ca-SDC, and Ti-SDC). The synthesized material characterized by using Raman Spectroscopy, UV-Visible spectroscopy, Fourier Transformation Infrared Radiation, Conductivity Measurement and Fuel Cell Performance.

Raman spectra reveal the material's structural change and vibration modes. It describes the kind of shifting that takes place in the prepared material. A red shift indicates a rise in wavelength, which shows a reduction in the distance between the valance band & conduction band & an increase in the size of the particles. A blue shift indicates a decreasing wavelength, which indicates

The synthesized sample's band gap and absorbance are detected by UV-visible. FTIR provides information on functional groups' existence in materials in addition to organic or inorganic behavior of manufactured materials. With the aid of EIS, the conductivity of materials may be computed. Using hydrogen as fuel improves the conductivity of materials by utilizing fuel cell performance at 500°C to 700°C temperature.

Bibliography

1. Laguna-Bercero, M. A. (2012). Recent advances in high temperature electrolysis using solid oxide fuel cells: A review. *Journal of Power sources*, *203*, 4-16.
2. Wang, Y., Song, Y., & Xia, Y. (2016). Electrochemical capacitors: mechanism, materials, systems, characterization and applications. *Chemical Society Reviews*, *45*(21), 5925-5950.
3. Peng, T., Kellens, K., Tang, R., Chen, C., & Chen, G. (2018). Sustainability of additive manufacturing: An overview on its energy demand and environmental impact. *Additive Manufacturing*, *21*, 694-704.
4. Singhal, S. C. (2000). Advances in solid oxide fuel cell technology. *Solid state ionics*, *135*(1-4), 305-313.
5. Sievi, G., Geburtig, D., Skeledzic, T., Bösmann, A., Preuster, P., Brummel, O., ... & Wasserscheid, P. (2019). Towards an efficient liquid organic hydrogen carrier fuel cell concept. *Energy & environmental science*, *12*(7), 2305-2314.
6. Staffell, I., Dodds, P., Scamman, D., Abad, A. V., Dowell, N. M., Ward, K., ... & Ekins, P. (2017). *The role of hydrogen and fuel cells in future energy systems*. Hydrogen and Fuel Cell Research Hub.
7. Raza, R., Abbas, G., Wang, X., Ma, Y., & Zhu, B. (2011). Electrochemical study of the composite electrolyte based on samaria-doped ceria and containing yttria as a second phase. *Solid State Ionics*, *188*(1), 58-63.
8. Supapo, K. R. M., Lozano, L., Tabañag, I. D. F., & Querikiol, E. M. (2021). A Geospatial Approach to Energy Planning in Aid of Just Energy Transition in Small Island Communities in the Philippines. *Applied Sciences*, *11*(24), 11955.
9. Kötz, R., & Carlen, M. J. E. A. (2000). Principles and applications of electrochemical capacitors. *Electrochimica acta*, *45*(15-16), 2483-2498.
10. Jiang, H., Zhao, T., Ma, J., Yan, C., & Li, C. (2011). Ultrafine manganese dioxide nanowire network for high-performance supercapacitors. *Chemical communications*, *47*(4), 1264-1266.
11. Jiang, H., Yang, L., Li, C., Yan, C., Lee, P. S., & Ma, J. (2011). High–rate electrochemical capacitors from highly graphitic carbon–tipped manganese

oxide/mesoporous carbon/manganese oxide hybrid nanowires. *Energy & Environmental Science*, *4*(5), 1813-1819.

12. Shaqsi, A. Z. A., Sopian, K., & Al-Hinai, A. (2020). Review of energy storage services, applications, limitations, and benefits. *Energy Reports*, *6*, 288-306.
13. Gür, T. M. (2020). Perspectives on oxygen-based coal conversion towards zero-carbon power generation. *Energy*, *196*, 117074.
14. Nicholas, J. D. (2013). Highlights from the 2013 National Science Foundation Solid Oxide Fuel Cell Promise, Progress, and Priorities (SOFC-PPP) Workshop. *The Electrochemical Society Interface*, *22*(4), 49.
15. Chasta, G., Himanshu, & Dhaka, M. S. (2022). A review on materials, advantages, and challenges in thin film based solid oxide fuel cells. *International Journal of Energy Research*, *46*(11), 14627-14658.
16. Kirubakaran, A., Jain, S., & Nema, R. K. (2009). A review on fuel cell technologies and power electronic interface. *Renewable and sustainable energy reviews*, *13*(9), 2430-2440.
17. Cook, B. (2002). Introduction to fuel cells and hydrogen technology. *Engineering Science & Education Journal*, *11*(6), 205-216.
18. Larminie, J., Dicks, A., & McDonald, M. S. (2003). *Fuel cell systems explained* (Vol. 2, pp. 207-225). Chichester, UK: J. Wiley.
19. Kirubakaran, A., Jain, S., & Nema, R. K. (2009). A review on fuel cell technologies and power electronic interface. *Renewable and sustainable energy reviews*, *13*(9), 2430-2440.
20. Farooque, M., & Maru, H. C. (2001). Fuel cells-the clean and efficient power generators. Proceedings of the IEEE, 89(12), 1819-1829.
21. Stambouli, A. B., & Traversa, E. (2002). Fuel cells, an alternative to standard sources of energy. *Renewable and sustainable energy reviews*, *6*(3), 295-304.
22. O'Sullivan, J. B. (1999, July). Fuel cells in distributed generation. In *1999 IEEE Power Engineering Society Summer Meeting. Conference Proceedings (Cat. No. 99CH36364)* (Vol. 1, pp. 568-572). IEEE.
23. Raza, R. (2011). *Functional nanocomposites for advanced fuel cell technology and polygeneration* (Doctoral dissertation, KTH Royal Institute of Technology).

24. Gür, T. M. (2020). Perspectives on oxygen-based coal conversion towards zero-carbon power generation. *Energy*, *196*, 117074.
25. Kirubakaran, A., Jain, S., & Nema, R. K. (2009). A review on fuel cell technologies and power electronic interface. *Renewable and sustainable energy reviews*, *13*(9), 2430-2440.
26. Ormerod, R. M. (2003). Solid oxide fuel cells. *Chemical Society Reviews*, *32*(1), 17-28.
27. Raza, R. (2011). *Functional nanocomposites for advanced fuel cell technology and polygeneration* (Doctoral dissertation, KTH Royal Institute of Technology).
28. Stambouli, A. B., & Traversa, E. (2002). Solid oxide fuel cells (SOFCs): a review of an environmentally clean and efficient source of energy. *Renewable and sustainable energy reviews*, *6*(5), 433-455.
29. Prakash, B. S., Kumar, S. S., & Aruna, S. T. (2014). Properties and development of Ni/YSZ as an anode material in solid oxide fuel cell: A review. *Renewable and Sustainable Energy Reviews*, *36*, 149-179.
30. Lee, J. G., Park, J. H., & Shul, Y. G. (2014). Tailoring gadolinium-doped ceria-based solid oxide fuel cells to achieve 2 W cm− 2 at 550 C. *Nature communications*, *5*(1), 4045.
31. Mahato, N., Banerjee, A., Gupta, A., Omar, S., & Balani, K. (2015). Progress in material selection for solid oxide fuel cell technology: A review. *Progress in Materials Science*, *72*, 141-337.
32. Gorte, R. J., & Vohs, J. M. (2009). Nanostructured anodes for solid oxide fuel cells. *Current Opinion in Colloid & Interface Science*, *14*(4), 236-244.
33. Zakaria, Z., Awang Mat, Z., Abu Hassan, S. H., & Boon Kar, Y. (2020). A review of solid oxide fuel cell component fabrication methods toward lowering temperature. *International Journal of Energy Research*, *44*(2), 594-611.
34. Adams, T. A., Nease, J., Tucker, D., & Barton, P. I. (2013). Energy conversion with solid oxide fuel cell systems: A review of concepts and outlooks for the short-and long-term. *Industrial & Engineering Chemistry Research*, *52*(9), 3089-3111.

35. Saadabadi, S. A., Thattai, A. T., Fan, L., Lindeboom, R. E., Spanjers, H., & Aravind, P. V. (2019). Solid Oxide Fuel Cells fuelled with biogas: Potential and constraints. *Renewable Energy*, *134*, 194-214.
36. Jabbari, M., Bulatova, R., Tok, A. I. Y., Bahl, C. R. H., Mitsoulis, E., & Hattel, J. H. (2016). Ceramic tape casting: A review of current methods and trends with emphasis on rheological behaviour and flow analysis. *Materials Science and Engineering: B*, *212*, 39-61.
37. Ramesh, S. (2023). Structural, optical and electrical properties of M0. 025Sm0. 175Ce0. 8O2-δ: an electrolyte for IT-SOFCs. *Journal of Taibah University for Science*, *17*(1), 2177064.
38. Altaf, F., Batool, R., Gill, R., Abbas, G., Raza, R., Khan, M. A., ... & Ahmad, M. A. (2019). Synthesis and characterization of co-doped ceria-based electrolyte material for low temperature solid oxide fuel cell. *Ceramics International*, *45*(8), 10330-10333.
39. Ning, Z., Milin, Z., Fucheng, X., Cheng, W., Zhixiang, L., & Zongqiang, M. (2012). Fabrication and characterization of anode support low-temperature solid oxide fuel cell based on the samaria-doped ceria electrolyte. *International journal of hydrogen energy*, *37*(1), 797-801.
40. Khan, M. A., Raza, R., Lima, R. B., Chaudhry, M. A., Ahmed, E., & Abbas, G. (2013). Comparative study of the nano-composite electrolytes based on samaria-doped ceria for low temperature solid oxide fuel cells (LT-SOFCs). *International journal of hydrogen energy*, *38*(36), 16524-16531.
41. Rafique, A., Ahmad, M. A., Shakir, I., Ali, A., Abbas, G., Javed, M. S., ... & Raza, R. (2020). Multioxide phase-based nanocomposite electrolyte (M@ SDC where M= Zn2+/Ba2+/La3+/Zr2+/Al3+) materials. *Ceramics International*, *46*(5), 6882-6888.
42. Liu, M., Ding, D., Bai, Y., He, T., & Liu, M. (2012). An efficient SOFC based on samaria-doped ceria (SDC) electrolyte. *Journal of the electrochemical society*, *159*(6), B661.
43. Zheng, Y., He, S., Ge, L., Zhou, M., Chen, H., & Guo, L. (2011). Effect of Sr on Sm-doped ceria electrolyte. *international journal of hydrogen energy*, *36*(8), 5128-5135.

44. Ji, Y., Liu, J., He, T., Wang, J., & Su, W. (2005). The effect of Pr co-dopant on the performance of solid oxide fuel cells with Sm-doped ceria electrolyte. *Journal of Alloys and Compounds*, *389*(1-2), 317-322.
45. Cheng, J., Tian, C., & Yang, J. (2019). Effects of Fe 2 O 3 addition on the electrical properties of SDC solid electrolyte ceramics. *Journal of Materials Science: Materials in Electronics*, *30*, 16613-16620.
46. Hussain, S., Li, Y., Mustehsin, A., Ali, A., Thebo, K. H., Ali, Z., & Hussain, S. (2021). Synthesis and characterization of ZnO/samarium-doped ceria nanocomposites for solid oxide fuel cell applications. *Ionics*, *27*(11), 4849-4857.
47. Xia, M., Jia, L., Li, J., Liu, Y., Wang, X., Chi, B., ... & Jian, L. (2018). Effects of co-doped barium cerate additive on morphology, conductivity and electrochemical properties of samarium doped ceria electrolyte for intermediate temperature solid oxide fuel cells. *International Journal of Hydrogen Energy*, *43*(33), 16293-16301.
48. Tamm, K., Raudsepp, R., Kanarbik, R., Möller, P., Nurk, G., & Lust, E. (2013). Investigation of microstructure of Sr-doped lanthanum vanadium oxide anode based on SDC electrolyte. *ECS Transactions*, *57*(1), 1185.
49. Shen, C. T., Lee, K. R., Hsieh, Y. P., Lee, S. W., Chang, J. K., Jang, S. C., & Tseng, C. J. (2019). Effects of TiO2 and SDC addition on the properties of YSZ electrolyte. *International Journal of Hydrogen Energy*, *44*(56), 29426-29431.
50. Downes, A., & Elfick, A. (2010). Raman spectroscopy and related techniques in biomedicine. *Sensors*, *10*(3), 1871-1889.
51. Rocha, F. S., Gomes, A. J., Lunardi, C. N., Kaliaguine, S., & Patience, G. S. (2018). Experimental methods in chemical engineering: Ultraviolet visible spectroscopy—UV-Vis. *The Canadian Journal of Chemical Engineering*, *96*(12), 2512-2517.
52. Fadlelmoula, A., Pinho, D., Carvalho, V. H., Catarino, S. O., & Minas, G. (2022). Fourier transform infrared (FTIR) spectroscopy to analyse human blood over the last 20 years: a review towards lab-on-a-chip devices. *Micromachines*, *13*(2), 187.
53. Schultz, J. F. (2021). *Probing Nanostructures on Surfaces with Scanning Tunneling Microscopy and Tip-Enhanced Raman Spectroscopy* (Doctoral dissertation, University of Illinois at Chicago).

54. Wheeler, D. W., & Khan, I. (2014). A Raman spectroscopy study of cerium oxide in a cerium–5 wt.% lanthanum alloy. *Vibrational Spectroscopy*, *70*, 200-206.
55. Kainbayev, N., Sriubas, M., Virbukas, D., Rutkuniene, Z., Bockute, K., Bolegenova, S., & Laukaitis, G. (2020). Raman study of nanocrystalline-doped ceria oxide thin films. *Coatings*, *10*(5), 432.
56. Sovilj, S. P., Vučković, G., Babić, K., Matsumoto, N., Avramov-ivić, M., & Jovanović, V. M. (1994). Synthesis, characterization, structure and possible catalytic properties of cis-oxalato (1, 4, 8, 11-tetraazacyclotetradecane) cobalt (III) nitrate. *Journal of Coordination Chemistry*, *31*(2), 167-179.
57. Ullah, S., Kamran, M. A., Raheel, M., Alharbi, T., Ali, W., & Zou, B. (2023). Powering up the energy storage: Exploring the potential of Graphitic Carbon Nitride-Strontium Oxide Nanohybrid for next-generation energy and photocatalytic applications. *Journal of Energy Storage*, *72*, 108806.
58. Khalid, A., Ahmad, P., Alharthi, A. I., Muhammad, S., Khandaker, M. U., Iqbal Faruque, M. R., ... & Alotaibi, M. A. (2021). Unmodified Titanium Dioxide Nanoparticles as a Potential Contrast Agent in Photon Emission Computed Tomography. Crystals 2021, 11, 171.
59. Baillon, F., Provost, E., & Fürst, W. (2008). Study of titanium (IV) speciation in sulphuric acid solutions by FT-Raman spectrometry. *Journal of Molecular Liquids*, *143*(1), 8-12.
60. Heilala, B., Mäkinen, A., Nissinen, I., Nissinen, J., Mäkynen, A., & Perämäki, P. (2018). Evaluation of time-gated Raman spectroscopy for the determination of nitric, sulfuric and hydrofluoric acid concentrations in pickle liquor. *Microchemical Journal*, *137*, 342-347.
61. Amarsingh Bhabu, K., Theerthagiri, J., Madhavan, J., Balu, T., Muralidharan, G., & Rajasekaran, T. R. (2016). Cubic fluorite phase of samarium doped cerium oxide (CeO_2) 0.96 Sm 0.04 for solid oxide fuel cell electrolyte. *Journal of Materials Science: Materials in Electronics*, *27*, 1566-1573.
62. Kosacki, I., Rouleau, C. M., Becher, P. F., Bentley, J., & Lowndes, D. H. (2005). Nanoscale effects on the ionic conductivity in highly textured YSZ thin films. *Solid State Ionics*, *176*(13-14), 1319-1326.